ADVANCED ENERGY MATERIALS
www.advenergymat.de

Advances in Piezo-Phototronic Effect Enhanced Photocatalysis and Photoelectrocatalysis

Lun Pan, Shangcong Sun, Ying Chen, Peihong Wang, Jiyu Wang, Xiangwen Zhang, Ji-Jun Zou, and Zhong Lin Wang**

Direct conversion of solar light into chemical energy by means of photocatalysis or photoelectrocatalysis is currently a point of focus for sustainable energy development and environmental remediation. However, its current efficiency is still far from satisfying, suffering especially from severe charge recombination. To solve this problem, the piezo-phototronic effect has emerged as one of the most effective strategies for photo(electro)catalysis. Through the integration of piezoelectricity, photoexcitation, and semiconductor properties, the built-in electric field by mechanical stimulation induced polarization can serve as a flexible autovalve to modulate the charge-transfer pathway and facilitate carrier separation both in the bulk phase and at the surfaces of semiconductors. This review focuses on illustrating the trends and impacts of research based on piezo-enhanced photocatalytic reactions. The fundamental mechanisms of piezo-phototronics modulated band bending and charge migration are highlighted. Through comparing and classifying different categories of piezo-photocatalysts (like the typical ZnO, MoS_2, and $BaTiO_3$), the recent advances in polarization-promoted photo(electro)catalytic processes involving water splitting and pollutant degradation are overviewed. Meanwhile the optimization methods to promote their catalytic activities are described. Finally, the outlook for future development of polarization-enhanced strategies is presented.

1. Introduction

The storage/utilization of solar energy is a promising strategy to alleviate current disparities in energy shortage and environmental crisis. To this end, photo(electro)catalysis, which are the dominant chemical processes for hydrogen production, carbon dioxide reduction and pollutant treatment, are expected to realize direct solar conversion and satisfy the growing global energy demands.[1,2] Since the report of TiO_2 photoelectrode by Fujishima and Honda, numerous efforts have been concentrated on developing excellent semiconductor photocatalysts.[3] As illustrated in **Figure 1**, photocatalysis and photoelectrocatalysis generally involve three elemental steps: i) absorption of photons and generation of electron–hole pairs in semiconductor, ii) charge separation and migration from bulk to surface, and finally iii) surface redox reaction. One major difference between photocatalysis and photoelectrocatalysis is that the former usually occurs in a reaction solution with the photocatalysts suspended, while the latter system has two separate electrolytes respectively for reduction and oxidation reactions with external bias added for accelerating electron transfer (Figure 1). The performance of photocatalysts and photoelectrocatalysts (photoanode or photocathode) substantially rely on charge separation and transfer kinetics, and it is still greatly fallen short of the target values (a solar-to-hydrogen

Prof. L. Pan, S. Sun, Y. Chen, Prof. X. Zhang, Prof. J.-J. Zou
Key Laboratory for Green Chemical Technology of the Ministry of Education
School of Chemical Engineering and Technology
Tianjin University
Tianjin 300072, China
E-mail: jj_zou@tju.edu.cn
Prof. L. Pan, Prof. X. Zhang, Prof. J.-J. Zou
Collaborative Innovative Center of Chemical Science and Engineering
Tianjin 300072, China
Prof. P. Wang
School of Physics and Materials Science
Anhui University
Hefei, Anhui 230601, China
The ORCID identification number(s) for the author(s) of this article can be found under https://doi.org/10.1002/aenm.202000214.

DOI: 10.1002/aenm.202000214

Dr. J. Wang
State Key Laboratory of Power Transmission Equipment and System Security and New Technology
Chongqing University
Chongqing 400044, China
Prof. Z. L. Wang
Beijing Institute of Nanoenergy and Nanosystems
Chinese Academy of Sciences
Beijing 100083, China
E-mail: zhong.wang@mse.gatech.edu
Prof. Z. L. Wang
School of Material Science and Engineering
Georgia Institute of Technology
Atlanta, GA 30332, USA

efficiency of 10%) required for practical applications.[1] Therefore, several strategies, including heterojunction (type II, Z-scheme or p–n junctions) construction, metal or metal oxide decoration (such as Pt, RuO_2, NiO, CoO_x), and surface defect (V_O or V_{Ti}) engineering have been investigated to promote the charge migration on the surface of photo(electro) catalyst, but the advances in bulk charge separation are still lagging behind.[4,5]

Recently, the utilization of piezopotential and polarization charges has been demonstrated as an efficient tactic for improving transport behavior of electrons and holes both in bulk and on surface of photocatalysts. With the exploration of piezotronics, fast developments have been achieved in transistors, nanogenerators, LEDs and solar cells.[2,6] The coupling effect between piezoelectric polarization and photoelectric process is a subcategory of piezotronics, which is referred as piezo-phototronics for using piezoelectric polarization charges to tune/enhance optoelectronic processes.[7,8] This makes possible the engineering of charge-carrier characteristics at the heterojunction interface and bulk phase as a result of the built-in electric field, and provides a driving force for the transport of photoinduced charges (electrons/holes) in designed directions, facilitating their separation and suppressing their recombination.

The piezoelectric characteristic of semiconductors is originated from their non-centrosymmetric nature, and the typical materials include ZnO, GaN, InN, CdS, MoS_2, and some titanates.[9] Based on semiconductor physics and piezoelectric theory, various piezotronic metal–semiconductor contact and p–n junctions have been constructed. Piezotronic and piezo-phototronic effects here offer a basic guideline in modulating the coupling effect between piezopotential and semiconductor properties in energy harvesting.[10,11] The piezopotential and subsequent band level rearrangement are sensitively dependent on the continuity of occupied electronic states and the amount of free charges in piezoelectric semiconductors.[12]

As a new-emerging research field, piezo-phototronics has gone through rapid development since it was first proposed by Wang's group in 2010.[13] And the number of related publications increases exponentially, and the current average citations per item (published SCI papers) is 32.2 (up to January 2020, from Web of Science database), which indicates that piezo-phototronic process is attracting intensive interests in energy and environment science under current global energy crisis. Some reviews related to piezotronics and piezo-phototronics have been published,[7,9,14–16] but few of them handle with the principle role of piezo-enhanced photo(electro)catalysis in both water splitting and organic pollution treatment, as well as the functional mechanism of piezo-phototronics in water splitting process. In this review, we highlight the fundamental mechanism of piezotronics/piezo-phototronics modulated band bending and charge migration. And recent advances in polarization-promoted photo(electro)catalytic processes involving water splitting and pollutant degradation will be overviewed and the optimization methods for promoting their catalytic activities will be described. Finally, an outlook for the future development of polarization-enhanced strategies is presented.

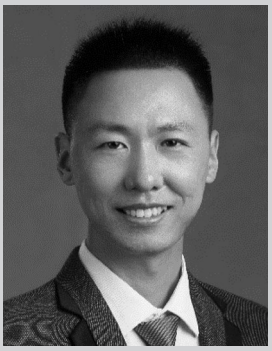

Lun Pan received his B.S. and Ph.D. degrees from the School of Chemical Engineering & Technology, Tianjin University, China, in 2009 and 2014, respectively. He became an associate professor in Tianjin University in 2018. His research interests mainly focus on the design and synthesis of functional photocatalysts; their related modulation of morphology, facets, and surface defects; and their applications in photocatalysis, such as photocatalytic isomerization, hydrogen generation, and environmental remediation.

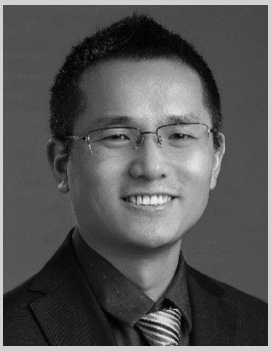

Ji-Jun Zou received his B.S., M.S., and Ph.D. degrees from Tianjin University in 2000, 2002, and 2005, respectively. He became a full professor in Tianjin University from 2013. His research interests mainly surround nanostructured materials for photo/electrocatalysis, fuel processing, and biomass conversion.

Zhong Lin Wang is the Hightower Chair in Materials Science and Engineering and Regents' Professor at Georgia Tech, and the Chief Scientist and Director of the Beijing Institute of Nanoenergy and Nanosystems, Chinese Academy of Sciences. His discovery and breakthroughs in developing nanogenerators and self-powered nanosystems establish the principle and technological road map for harvesting mechanical energy from environmental and biological systems for powering personal electronics and future sensor networks. He pioneered the field of piezotronics and piezo-phototronics.

2. Fundamentals of Piezo-Phototronic Effect on Photoinduced Catalysis

2.1. Piezopotential, Piezotronics, and Piezo-Phototronics

Piezoelectric effect is a coupling of mechanics and electric polarization. When a dielectric material is deformed through an applied force along its asymmetry direction, the positive and negative charges are generated on two opposite surfaces. The

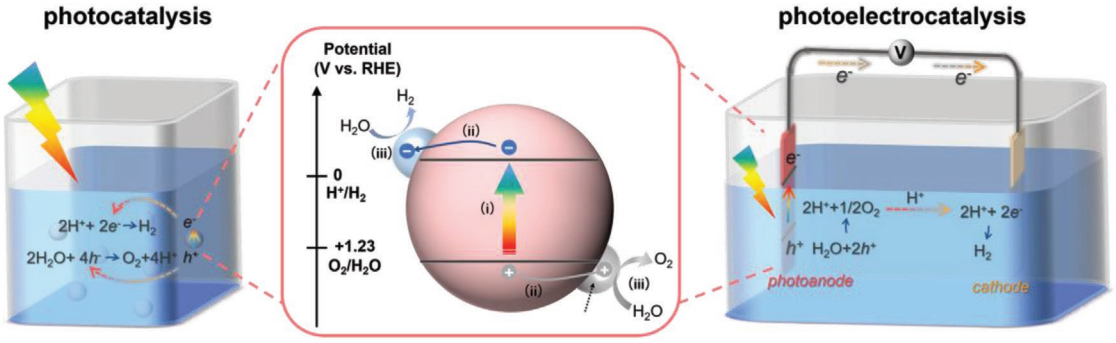

Figure 1. Schematic diagram of photocatalytic and photoelectrocatalytic water splitting processes.

lack of central symmetry in crystal gives rise to piezoelectricity, and the polarity of charge also changes along with the variation in direction of applied force.[14,17] Several representatives of third generation semiconductors, such as GaN and ZnO, have piezoelectric properties along their *c*-axis.[12,18] As a typical example, the wurtzite-structured ZnO (space group $P6_3mc$) usually possesses a large anisotropic property. The centers of positive Zn^{2+} cations and negative O^{2-} anions are overlapped with each other, and no polarization can be detected in the normal crystal. However, the two centers shift reversely when external strain is applied, leading to a dipole polarization (ionic charges) together with a built-in electric field (**Figure 2**a).[9] Such inner piezopotential keeps existence with the bearing of stress, which is mainly determined by the strength and direction of applied strain. A potential distributed along the stress direction is generated after dipole moment superposition occurs in the whole cells, which is the so-called piezopotential. For example, in a *c*-axis ZnO nanowire (space group $P6_3mc$) with length of 1.2 µm and hexagonal side length of 100 nm (Figure 2b), a tensile force of 85 nN creates a potential drop of ≈0.4 V between the two ends (Figure 2c). Some other cases are summarized in Figure 2d–g, which further confirm that the distribution of piezoelectric potential together with deformation shape is highly dependent on the strain force (including stretching force, compressing force, and twist force).[19]

The coupling of piezoelectric polarization and semiconductor properties (such as electronic transport and photoexcitation) also gives rise to superior synergetic effects, which offers feasible means of manipulating charge transport, recombination or separation through the application of external strain. Piezotronics is based on the piezoelectric properties by using the effect of piezopotential created in the crystal for promoting the carrier transport characteristics, which was first introduced by Wang et al. in 2006 and 2007.[20] Since then, significant progresses have been made in research such as nanogenerators, strain sensors, piezotronic field-effect transistors, solar cells, light-emitting diodes, strain-gated vertical nanowire arrays, and other devices.[10,21] Afterward, the concept of piezo-phototronics was first proposed by Prof. Wang in 2010.[13] Piezo-phototronics mainly focuses on modulating piezoelectric charges/piezopotential to tune the charge migration behaviors (separation, transportation, and recombination) and redox kinetics, which is simultaneously based on a coupling construction of semiconducting, photoexciting, and piezoelectric properties.[7,13,16,22] Moreover, the discontinuity in local band structure and accompanying band alignment are decisive to these intrinsic characteristics,[7] and understanding of interfacial band structure and properties in semiconductor is important for practical applications.

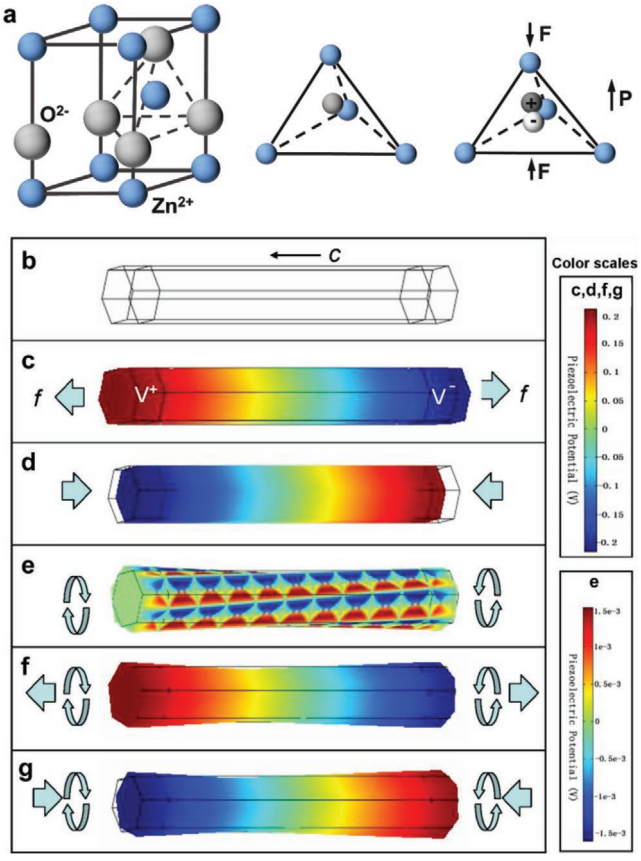

Figure 2. a) Schematic illustrations of atoms and charges distribution in the unit cell of wurtzite-structured ZnO, where F and P represent the applied stress and the induced electric dipole moment, respectively. Reproduced with permission.[16] Copyright 2012, Wiley-VCH. b) An unstrained ZnO nanowire grown along *c*-axis with a length of 1.2 µm and a hexagonal side length of 100 nm. Two ends of the nanowire are assumed to be surrounded by electrodes for a length of 100 nm. 3D views of the piezoelectric potential distribution together with deformation shape for the nanowire c) at a stretching force of 85 nN, d) at a compressing force of 85 nN, e) at a twist force pair of 60 nN, f) at a combination of 85 nN stretching force and 60 nN twist force, g) at a combination of 85 nN compressing force and 60 nN twist force. Reproduced with permission.[19] Copyright 2009, American Institute of Physics.

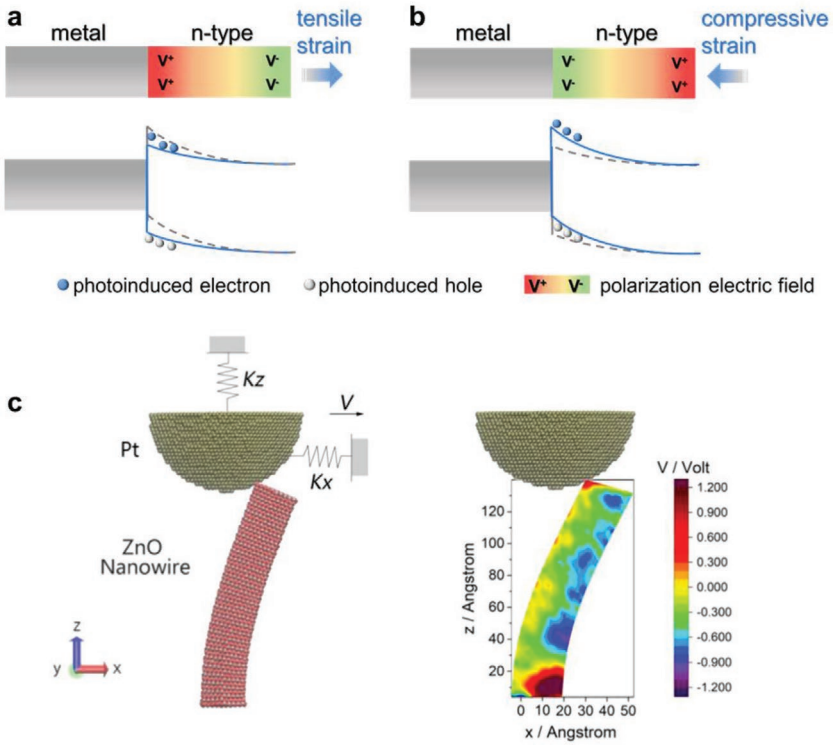

Figure 3. Schematic illustrations of piezotronic effect in metal–semiconductor contact under a) tensile and b) compressive strains (the gray dashed line represents the initial band edge without strain while the blue solid line represents the band edge under strain). Reproduced with permission.[16] Copyright 2012, Wiley-VCH. c) Schematic molecular dynamics simulation of the mechanical bending of a ZnO nanowire by a metal tip (left) and the associated piezopotential distribution within the nanowire (right). Reproduced with permission.[24] Copyright 2018, Elsevier.

In summary, there are two typical features of piezotronics and piezo-phototronics: i) piezoelectric materials usually needs an external mechanical stimuli (or heat for pyroelectric materials) to generate polarization charges; ii) the accompanying built-in electric field controls the migration of carriers in space charge region and affects redox kinetics at surface of metal–semiconductor contacts or semiconductor–semiconductor heterojunctions.[10,14]

2.2. Effect of Piezopotential on Metal–Semiconductor Contacts

Carrier transport characteristics through metal–semiconductor contact is important in both photocatalysis and photoelectrocatalysis. As shown in **Figure 3**a, when a n-type semiconductor is in contact with a metal such as Pt (normally with larger work function), the free electrons of semiconductor will flow to metal through the interface until achieving Fermi level alignment, leading to an upward band bending of the semiconductor and a corresponding Schottky barrier in space charge region. The height of Schottky barrier usually depends on the work function difference between semiconductor and metal, and only the photoinduced electron whose energy surpasses the Schottky barrier is able to step over the interface and participate in surface reaction. Specifically, for piezoelectric semiconductors, the Schottky barrier height can be effectively modulated by piezotronics effect. Either positive or negative polarization charges are induced through applying strain, leading to a change in interfacial band level.

Considering a metal/n-type semiconductor junction as example (Figure 3a,b), if the *c*-axis of semiconductor is oriented to the metal, a tensile strain will create positive polarization charges to attract free electrons at interface, downshift the band edge and reduce the barrier height, which is beneficial to electron migration. While a compressive strain induces negative charges to repulse electrons, uplift the band edge and increase the barrier height, resulting in a declined electron transfer at interface (from semiconductor to metal). Therefore, it can be seen that the piezoelectric polarization charges function as a two-way valve for tuning the electronic transport properties across interface. The strength of piezoelectric effect is positively related to the ratio of junction resistance to the bulk resistance. For example, considering 1D n-type piezotronic semiconductor with ideal Ohmic contacts at the source and drain, the current through metal–semiconductor interface exhibits an exponential function of the local polarization charge, which further depends on applied strain.[23] Therefore, the charge transfer property can be controlled by either the strength or the sign (tensile vs compressive) of imposed strain.

Computational modeling of metal–semiconductor contacts is also crucial for in-depth understanding of the structure and dynamics at piezotronics interface. Recently, Zhu et al. carried out molecular dynamics (MD) simulations to analyze the piezoelectric and mechanical properties of a bending Pt/ZnO nanowire interface, as shown in Figure 3c.[24] Ionic charges for Zn and O in ZnO were used to calculate the distribution of piezopotential in a grid-point matrix. The results show that there is always a positive piezopotential existing at the Pt/ZnO contacts, while the overall potential distribution along the *c*-axis of ZnO nanowire is not a constant; lateral friction and normal contact forces exhibit quite similar features during repeated forward–backward scans, implying a robust stability of piezoelectric properties. Moreover, the Schottky barrier height at metal/ZnO contacts depends on the size of contacts and the mechanical stability at interface during repeated external loadings.[10]

2.3. Effect of Piezopotential on p–n (or Type-II) and Z-Scheme Junction Contacts

The nature of piezotronics lies in the tuning effect of piezoelectric polarization on semiconductor behaviors. In most semiconductor devices, the formation of junctions at material

interface is usually an essential part for realizing its functionality. The corresponding alignment of Fermi level also induces an interfacial energy barrier when two kinds of semiconductors with different work functions are brought into contact. For the same reason as metal–semiconductor contacts, the barrier height can be manipulated accordingly if polarization charges are introduced. It is worth noting that, for piezoelectric semiconductors spontaneously grow along their polar directions, the distribution of the piezoelectric field is along the semiconducting channel.

Piezotronic effect can take place at n–n junctions, p–p junctions as well as p–n junctions (also including type-II and Z-scheme heterojunctions). For example, the most important character of a p–n junction is the presence of depletion region due to interfacial diffusion of holes and electrons.[17] Such strong built-in electric field generally plays a decisive role in regulating the interfacial charge migration, whose configuration, in addition, can be manipulated by introducing piezotronic effect via external strain on the junctions easily.

In the case of a 1D n-type piezotronic semiconductor contacted with a non-piezoelectric p-type counterpart (**Figure 4**a). A tensile strain on the junctions leads to positive piezoelectric charges on the n-type semiconductor, which attracts a portion of transporting electrons nearby and results a downward band-edge bending. The positive polarized charges thereby tune the space charge region moving toward the p-type semiconductor, which obstructs the transfer of carriers.[9,25] By contrast, when negative polarization charges are induced by compressive strain at the interface (Figure 4b), electrons are repelled, leading to an upward bending of the band edge. This will lead to an enhanced transportation of photoinduced carriers.[9] Similar piezotronics effect can be found for type-II heterojunctions.

Another case is for the junctions with Z-scheme matched band structures, like Z-scheme ZnO/WO_3 nanorod arrays.[26] For a typical Z-scheme structure, the left semiconductor possesses higher conduction band (CB) and valance band (VB) levels, as well as higher Fermi level (E_F) than those of the right one. When they contact with each other, the alignment of Fermi level leads to an upward bending of the left semiconductor and a downward bending of the right one (see the gray dashed line of Figure 4c). Therefore, the formed interface electric field will facilitate the recombination of holes from the left semiconductor and electrons from the right one, maintaining highly reductive electrons and oxidative holes on the left and right semiconductors, respectively.[4,27] In this case, if one semiconductor (using the right one as an example) exhibits piezotronics property, the Z-scheme electronic transfer can be modulated. As shown in Figure 4c, the generated positive polarization charges by a tensile strain will enhance the downward bending of the right semiconductor, and further accelerate the recombination of holes (from the left VB) and electrons (from the right CB). By contrast, a compressive strain will produce negative charges, which suppress the Z-scheme charge transfer (Figure 4d).

Therefore, the piezoelectric effect can be rationally tuned to enhance the p–n (or type II) and Z-scheme charge-transfer processes. In addition, the carrier transported across the junction is highly dependent on the polarization charges (calculated from an abrupt junction mode), which can be tuned by both the magnitude and sign of the strain.[23]

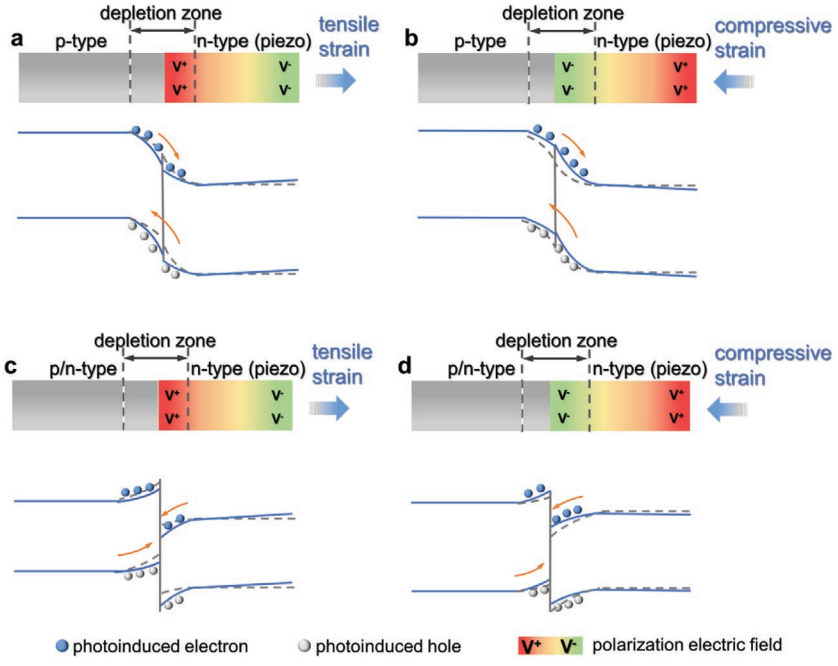

Figure 4. Schematic illustrations of the piezotronic effect in p–n (or type-II) junction under a) tensile and b) compressive strains. Reproduced with permission.[16] Copyright 2012, Wiley-VCH. Piezotronic effect in Z-scheme (p–n) junction under c) tensile and d) compressive strains. The gray dashed line represents the initial band edge without strain while the blue solid line represents the band edge under strain.

2.4. Mechanisms of Piezo-Phototronic Effect Enhanced Photo(Electro)Catalytic Processes

Photocatalytic and photoelectrocatalytic processes have been receiving extensive attention in solar energy conversion.[23] In a typical photocatalytic system, under the illumination by light with photons energy equal to or higher than the bandgap of photocatalyst, the electrons will be excited from VB to CB, with the holes generated on VB. The electrons and holes will then migrate to the semiconductor/solution interface and participate in reduction and oxidation reactions, respectively (Figure 1). While a photoelectrocatalytic system is generally consisted of electrodes (at least one photoelectrode, photoanode or photocathode), aqueous electrolyte and external electric wire connecting the photoelectrode with counter electrode. Under irradiation, electrons from the photoanode will transfer through the external circuit to the surface of cathode for reduction half reaction (like hydrogen evolution reaction, HER), meanwhile the holes diffuse to anode surface to assist oxidation reaction (like oxygen evolution reaction, OER). Accordingly, for the

whole process of photocatalysis or photoelectrocatalysis, light absorption, charge separation and surface reaction are three fundamental steps, and the overall solar conversion efficiency (or quantum efficiency) is dependent on the cumulative efficiency of above three steps.

The capability of piezoelectric photocatalysis to simultaneously utilize solar energy and mechanical energy, which may break a new ground for the design of energy conversion materials toward harvesting discrete ambient energy, has gained tremendous attention recently. Meanwhile such approach is more efficient in promoting the bulk charge separation than other common approaches like cocatalyst loading on photocatalysts.[28] Moreover, the piezo-induced internal electric field also modulates the surface redox reactions, which are the final steps during the photo(electro)catalytic processes. As shown in **Figure 5**a,b, when a common semiconductor is in contact with the electrolyte solution, the photoinduced free carriers move toward electrolyte solution through the interface, leading to an upward bending on the surface of photocatalyst. This kind of band bending acts as a barrier of electron transfer for surface reduction reaction, but facilitates hole transfer for oxidation reaction. Importantly, if the photocatalyst is a piezoelectric semiconductor, external strain can generate a spontaneous internal electric field due to the presence of polarized charges. The surface energy level with positive polarization charge is downward bent throughout the domain (Figure 5c), such that the surface will be at a higher potential compared with before. This

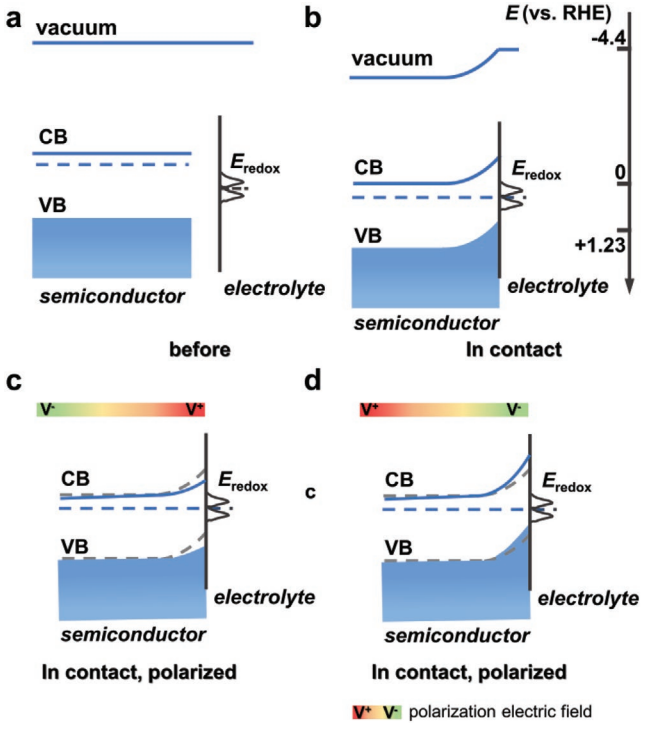

Figure 5. Band structure diagrams of semiconductor/electrolyte interface based on n-type semiconductor in photocatalysis, a) before and b) after the contact as well as further under c) positive or d) negative polarizations. The gray dashed line represents the initial band edge without strain while the blue solid line represents the band edge under strain. Reproduced with permission.[30] Copyright 2019, Elsevier.

case is beneficial for electron migration to the electrolyte (but slightly reduces the reductive potential), and its oxidation ability is further enhanced. By contrast, with negative polarization charges, a potential is gained across the domain and the band is upward bent, thus the surface is at a lower potential than before (Figure 5d). And in this case, the transfer kinetics of photoinduced electrons is suppressed for the increased energy barrier, while the hole transfer will be facilitated (but slightly reduces the oxidative potential). In total, determined by the strength of internal electric field, different degrees of band bending obtained by tuning the direction/strength of applied strain can result in varied transfer kinetics of surface charges. Meanwhile the driving force (redox potential of charges) toward the goal reaction in certain electrolyte solution can also be manipulated. Besides, recent study has clarified that the photoinduced electrons and holes in piezoelectric semiconductors are major candidates for reaction, meanwhile polarization charges can modulate the band bending to facilitate the transfer photoinduced charges.[29]

The basic photoelectrocatalytic process is illustrated in **Figure 6** by considering a n-type semiconductor in a loop current. The photoelectrode absorbs light and excites electrons from VB to CB, generating electron–hole pairs. The electrons in CB tend to move toward the semiconductor side because of the upward bent band in the interface between semiconductor and electrolyte, and then transport through the external circulate to the counter electrode (cathode, usually Pt wire), while the holes in VB directly drift toward the electrolyte (Figure 6a). However, only the holes with higher oxidation potential than the redox potential of electrolyte are able to transfer through the semiconductor–electrolyte interface and participate in oxidation reaction. Otherwise no charge exchange or redox process will be proceeded.

As for a piezoelectric semiconductor (normally the photoanode), if a tensile strain is applied, the side directly interfacing with the electrolyte will have a negative piezopotential, leading to an upward bending of the band edge. Thus, the steeply lifted CB makes it easier for electrons to migrate from the electrolyte side to the indium-tin-oxide (ITO) side (then to the external electric wire), and the reduced VB position at semiconductor/electrolyte interface efficiently reduces the local resistance or threshold voltage for surface oxidation reaction (Figure 6b). All these factors are favorable for enhancing photoelectrocatalytic process. In comparison, when a compressive strain is imposed (Figure 6c), the positive piezopotential lowers and flattens the band edges at semiconductor/electrolyte interface, which will reduce the driving force of electron–hole separation and increases threshold voltage and local resistance (although the oxidative potential can be enhanced), usually retarding the redox efficiency.

Structure–activity correlation is always a central theme in catalysis. The material physical properties, like crystal phase, morphology, dimension, etc., can obviously affect the piezophototronic response. 1) Crystal phase. For example, Liu et al. reported that orthorhombic $KNbO_3$ nanowire is about two times more active than its monoclinic counterparts in aqueous rhodamine B (RhB) and *N*-de-ethylation degradation, by means of both experiments and DFT calculations, for the higher 7.6% in the former;[31] 2) Shape/morphology (like nanoparticle,[32]

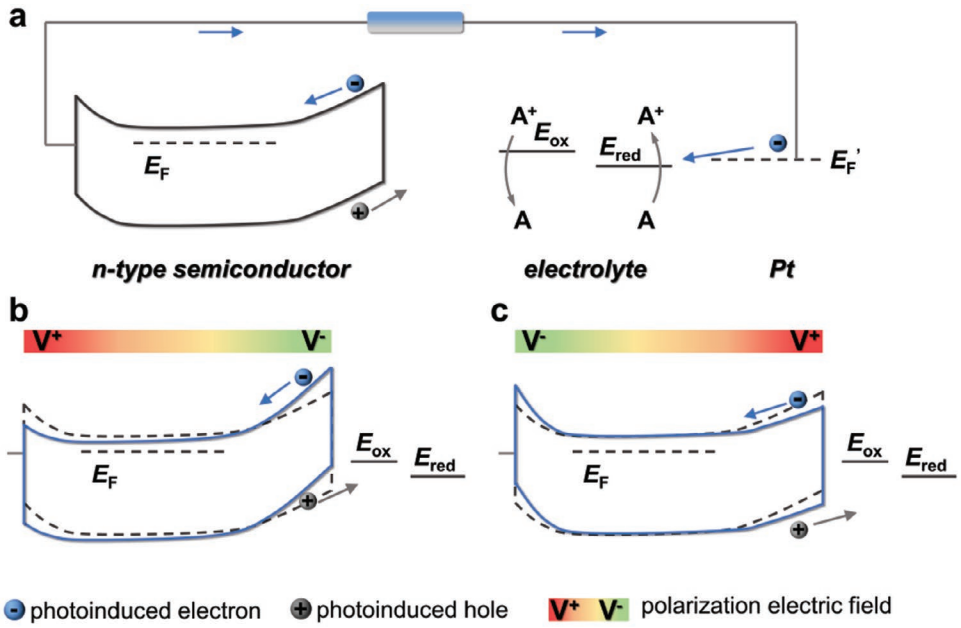

Figure 6. Piezo-phototronic effect on photoelectrocatalytic process (photoanode). a) Illustration of photoelectrocatalytic process a) without strain, b) under tensile strain and c) under compressive strain. The gray dashed line represents the initial band edge without strain while the blue solid line represents the band edge under strain. Reproduced with permission.[16] Copyright 2012, Wiley-VCH.

nanofiber,[33] nanowire,[14,34–36] nanorod,[37,38] nanoflower,[39] nanoplatelets,[40] microsphere, and nest-like hollow microsphere[30]). For example, Yu et al. has revealed that the piezo-polarization of $KNbO_3$ can be efficiently tuned by changing its poling configuration (nanosheets or nanocubes).[41] Owing to the larger piezo-response, $KNbO_3$ nanosheets exhibit better piezo-photocatalytic degradation efficiency compared to the nanocube counterparts. 3) Dimension and size. The dimensions (0D–3D) and sizes are also crucial to piezo-response and catalytic properties. Owing the 2D confinement and spontaneous breaking of inversion symmetry, 2D materials usually exhibit high piezo-phototronic actives.[42] Besides, although a larger specific surface area is usually preferable in catalysis, the change in piezopotential may cause different results. The physical properties affect not only the surface area but also the distribution and strength of built-in polarization electric field, which result in different catalytic activities. Therefore, attentions should be paid on analyzing/excluding the effect of material physical properties during catalyst design and characterization.

2.5. Theoretical Framework of the Photo(Electro)Catalytic Processes

Semiconductor physics and piezoelectric theory are generally utilized to analyze the piezo-phototronic effect.[16,23] Some basic fundamental equations including electrostatic, piezoelectric, current–density, and continuity functions are need to be balanced.[14]

Poisson equation describes the electrostatic behavior of charges in piezoelectric semiconductor

$$\nabla^2 \varphi_i = -\frac{\rho(\mathbf{r})}{\varepsilon_s} \tag{1}$$

where φ_i, $\rho(\mathbf{r})$ and ε_s are electric potential distribution, charge density distribution, and permittivity of the material, respectively.[43]

The current–density equations give the relationship among the charge densities, local fields and local currents

$$J_n = q\mu_n nE + qD_n \nabla n \tag{2}$$

$$J_p = q\mu_p pE - qD_p \nabla p \tag{3}$$

$$J_{cond} = J_n + J_p \tag{4}$$

where J_n and J_p are current densities of electrons and holes, q is electric charge quantity, μ_n and μ_p are mobilities of electrons and holes, n and p are concentrations of electrons and holes, E is electric field, D_n and D_p are diffusion coefficients for electrons and holes, and J_{cond} is total current density.

Continuity equations describe the charge transport properties under field

$$\frac{\partial n}{\partial t} = G_n - U_n + \frac{1}{q}\nabla \cdot J_n \tag{5}$$

$$\frac{\partial p}{\partial t} = G_p - U_p - \frac{1}{q}\nabla \cdot J_p \tag{6}$$

where G_n and G_p are electron and hole generation rates, U_n and U_p are recombination rates.

The piezoelectric polarization vector ($\boldsymbol{P}$) under a uniform external strain ($\boldsymbol{S}$) is

$$(\boldsymbol{P})_i = (\boldsymbol{e})_{ijk}\,(\boldsymbol{S})_{jk} \tag{7}$$

where $(\boldsymbol{e})_{ijk}$ is a third-order piezoelectric tensor.

The constituent equations are

$$\boldsymbol{\sigma} = \boldsymbol{c}_{\mathrm{E}}\,\boldsymbol{S} - \boldsymbol{e}^{T}\boldsymbol{E} \tag{8}$$

$$\boldsymbol{D} = \boldsymbol{e}\,\boldsymbol{S} + \boldsymbol{k}\boldsymbol{E} \tag{9}$$

where $\boldsymbol{\sigma}$ and $\boldsymbol{c_E}$ are stress tensor and elasticity tensor, $\boldsymbol{E}$, $\boldsymbol{D}$, and $\boldsymbol{k}$ are electric field, the electric displacement and dielectric tensor.

The above equations can be calculated with specific boundary conditions for various hybrid/hetero structures, which build the framework on theoretical calculations for enhancing catalytic properties through piezo-phototronic effect.[14,44] Considering a simple static cylindrical Wurtzite nanowire with uniform cross section of diameter $2a$ and length l, when the material elastic constants are approximated by an isotropic elastic modulus with Young modulus E and Poisson ratio ν, the electric potential φ has been solved as[44]

$$\varphi = \begin{cases} \dfrac{1}{8k_\perp}\dfrac{f_y}{I_{xx}E}\left[2(1+\upsilon)e_{15}+2\upsilon e_{31}-e_{33}\right]\left[\dfrac{k_0+3k_\perp}{k_0+k_\perp}\dfrac{r}{a}-\dfrac{r^3}{a^3}\right]a^3\sin\theta, r<a \\ \dfrac{1}{8k_\perp}\dfrac{f_y}{I_{xx}E}\left[2(1+\upsilon)e_{15}+2\upsilon e_{31}-e_{33}\right]\left[\dfrac{2k_\perp}{k_0+k_\perp}\dfrac{a}{r}\right]a^3\sin\theta, r\geq a \end{cases} \tag{10}$$

where f_y is the force applied uniformly on the top surface, I_{xx} is the cross-section area, k_0 is the permittivity in vacuum, $k_{ik}$is the dielectric constant. e_{kp} is the linear piezoelectric coefficient. Hereon, taking photo(electro)catalytic water splitting process as an example, whose efficiency can be indexed by applied bias photon-to-current efficiency (ABPE)

$$\mathrm{ABPE}\,(\%) = \frac{J_{\mathrm{ph}}\times(1.23-\varphi_{\mathrm{app}})}{I_{\mathrm{total}}}\times 100 \tag{11}$$

where J_{ph} is obtained photocurrent density, φ_{app} is the applied electric bias, I_{total} is light intensity.[5] When the external strain is applied on a piezoelectric material, the generated piezopotential can function as an additional φ, and the piezo-photoelectric ABPE′ is given as

$$\mathrm{ABPE}'\,(\%) = \frac{J_{\mathrm{ph}}\times\left(1.23-(\varphi_{\mathrm{app}}-\varphi)\right)}{I_{\mathrm{total}}}\times 100 \tag{12}$$

Obviously, the piezo-phototronic effect can enhance the efficiency of photo(electro)catalytic processes.

Moreover, the improvement of photo(electro)catalysis efficiency by the piezo-effect can also be determined by the potential-dependent electron lifetime (τ), which can be calculated from the following formula[45]

$$\tau = \frac{\boldsymbol{k}_{\mathrm{B}}\times T/e}{d\boldsymbol{V}_{\mathrm{OC}}/\mathrm{d}t} \tag{13}$$

where τ, k_{B}, T, e, and V_{OC} respectively represent potential-dependent electron lifetime, Boltzmann's constant, temperature, a single electron charge and open-circuit voltage corresponding to the time t. The piezo-photocatalysis will lead to the decrease of $\mathrm{d}V_{\mathrm{OC}}/\mathrm{d}t$, which will be finally reflected in the extension of τ.

3. General Approaches to Creating Piezopotential

As discussed above, an external or internal strain is necessary to induce piezopotential in piezoelectric materials. And the resulting specific morphological changes (bending or other deformations) in nanostructures induce electric potentials on their surfaces. Common approaches to creating piezopotential in photocatalytic and photoelectrocatalytic semiconductors include ultrasonic vibration, mechanical stirring, mechanical force, thermal expansion and some other methods, among which the former three are most widely adopted (**Figure 7**).[26,34,37,46–49]

Both the periodic acoustic pressure of ultrasonic wave and the extreme pressure formed by the collapse of acoustic cavitation walls affect the intensity of spontaneous electric potential. Under ultrasonic treatment, water generates active bubbles, which subsequently collapse and cause high local pressure (>100 MPa).[43,50] The strength of internal piezoelectric potential is easily altered by changing the applied stress from ultrasonic waves including the work power and frequency.[37] Accordingly, the ultrasonic vibration can induce deformation or strain on piezoelectric materials (like ZnO nanorod arrays, Figure 7a), which functions as alternating built-in electric field to separate charge carriers and belongs to piezocatalytic process.[37,46,51,52] For example, the piezoelectric field inside the ultrasonic assisted CuS/ZnO/CuS composited nanowire can drive the photoinduced electrons/holes to migrate along opposite directions.[50] Although ultrasonic vibration is the most widely adopted method in piezotronic photo(electro)catalysis, the unidirectional control of polarization electric field may be difficult since the bending or deformation direction of semiconductor can be easily changed under nondirective ultrasonication. In that case, the overall piezotronic effect may be somewhat counteracted.

Alternatively, the mechanical-stirring-induced pressure of water can also lead to the bending of piezo material as well as related piezopotential (Figure 7c).[47,53] The flow of electrolyte by simple stirring can apply continuous piezoelectric field in one direction, and the stirring rate and direction can be easily tuned.[26] Previous reports have demonstrated that the stirring rate and direction have a great influence on water splitting activity.[26] Therefore, mechanical stirring is a very facile and promising approach to generate piezopotential for photo(electro)catalysis. However, it is worth noting that both ultrasonic vibration and mechanical stirring can also accelerate the mass transfer during reaction, thus conducting control experiments and analyses is necessary to clarify the contribution of piezotronics in the promotion of photocatalytic activity. And the clarification of piezocatalysis or sonocatalysis is necessary.

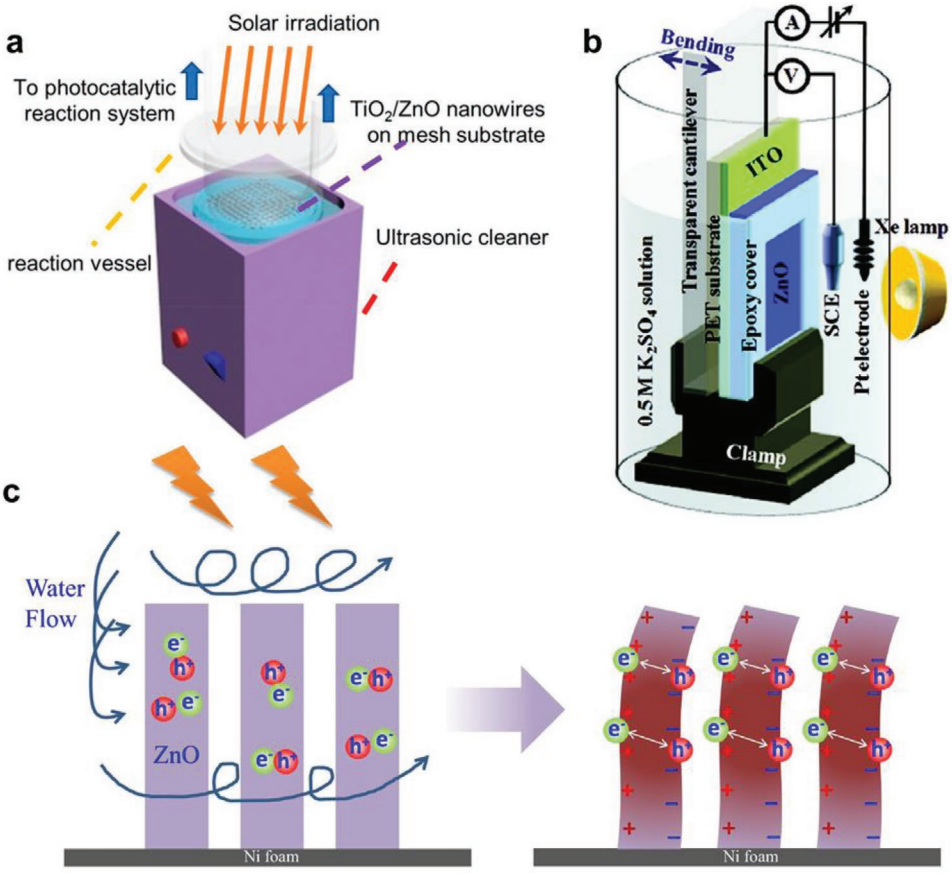

Figure 7. a) Sketch maps of ultrasonic-vibration-assisted photocatalytic reaction vessel. Reproduced with permission.[46] Copyright 2018, American Chemical Society. b) Setup for reaction cell equipped with a cantilever. Reproduced with permission.[54] Copyright 2015, American Chemical Society. c) Sketch maps turbulence-stirring induced deformation of nanorod. Reproduced with permission.[53] Copyright 2017, Elsevier.

In addition, physical bending has also been conducted by attaching cantilever to the piezoelectric material (that can be deformed to produce different strains on photoanode, Figure 7b),[54,55] applying periodical external force,[56] shake,[57] and other kinds of external forces.[34,48,49,58] Although these approaches are more complicated than ultrasonic and stirring methods, they provide precise models for a mechanical understanding of the correlation between piezotronics and reaction activity. Notably, Wang et al. introduce thermal internal stress to piezoelectric materials, through cooling hybrid photocatalysts from high temperature to room temperature with different rates based on the mismatched thermal expansion coefficients of the two materials, which is also a promising approach for piezo-photocatalytic/photoelectrocatalytic applications.[40]

4. Piezoelectric Polarization Promoted Photo(Electro)Catalysis

Piezoelectric property is widespread within the interior of noncentrosymmetric materials, such as piezoelectric, pyroelectric, ferroelectric, and nonlinear optical materials. Many materials, including metal oxides, metal sulfides/selenides, and oxysalts have been selected and utilized in piezoelectric process. Some of them possess both piezoelectric and photocatalytic properties, which simultaneously generate piezopotential and photoinduced charges. Some of them are piezoelectric and conductive, which introduce piezopotential and improve conductivity, which can serve as piezo-cocatalysts. And others are only piezoelectric and must cooperate with certain photocatalysts for the corresponding reactions.

4.1. Material with Synergetic Piezoelectric and Photocatalytic Properties

Direct generation of piezopotential in photocatalytic semiconductors is considered as the most facile strategy, and luckily some piezoelectric materials with bandgap of about 2.5–3.5 eV are also typical photocatalysts, enabling the synergetic coupling of these two properties. In this case, such semiconductor possesses both the piezoelectric and photocatalytic properties. It not only generates photoinduced electrons/holes under light illumination, but also provides strain-induced polarization charges to facilitate charge separation for surface reduction and oxidation (**Figure 8**). The typical materials include ZnO, CdS, metal niobates, etc.

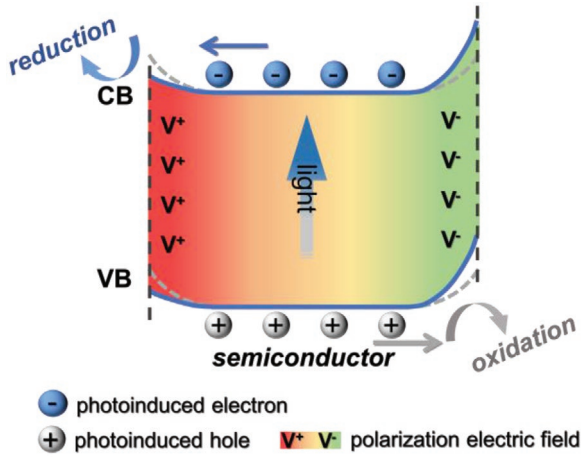

Figure 8. Schematic band structures of semiconductor with synergetic piezoelectric and photocatalytic properties. The gray dashed line represents the initial band edge without strain while the blue solid line represents the band edge under strain.

4.1.1. Zinc Oxide (ZnO)

Wurtzite zinc oxide (space group $P6_3mc$) semiconductor, with a high mobility of 210 $cm^2\ V^{-1}\ s^{-1}$ and a direct bandgap of 3.3 eV, is extensively investigated in photo(electro)catalytic processes.[59] Despite the efforts have been made toward band structure and surface structure engineering, ZnO based systems still suffer from low charge-separation efficiency. Since ZnO is also a typical piezoelectric material, the electronic band structure can be modulated by means of piezoelectric polarization. The generated piezopotential is in steady state as long as the strain remains, thus providing a continuous influence on semiconductor. Such an approach with the introduction of deformation and strain, taking advantage of the coupling between piezoelectric functionalities and semiconducting properties, has great potentials in enhancing the efficiencies of both water splitting and pollutant removal.

Water Splitting: The first report on direct water splitting by means of piezoelectric enhanced ZnO is in 2010. Hong et al. imposed ultrasonic waves to develop strain-induced electric polarization charges on ZnO microfibers, and demonstrated that the piezocatalytic process from polarized piezoelectric ZnO is robust in triggering the redox reaction (**Figure 9**a).[60] Since then, a series of piezo-enhanced ZnO catalysts have gained numerous interests and become one of the research hotspots, including bare ZnO, metal/ZnO composites, and ZnO-based heterojunctions.[37,50,54,56] For example, Chen et al. recently synthesized direct Z-scheme ZnO-WO_{3-x} (Zn-W) nanoarrays toward photoelectrochemical water splitting through a hydrothermal process, and demonstrated that the coupling of piezoelectricity (mechanical stirring) in ZnO (space group $P6_3mc$) can enhance Z-scheme property.[26] In this composite, the obvious piezo-polarization in ZnO increases its Fermi level toward CB and significantly facilitates the Z-scheme charge transfer between ZnO and WO_{3-x} (Figure 9b). Specifically, the optimized piezo Zn-W-5 shows a photocurrent of 3.38 mA cm^{-2} at 1.23 V versus RHE, which is 3.02 times higher than pure ZnO and 1.41 times higher than the strain-free Zn-W-5. The corresponding incident photon to current efficiency (IPCE) reaches to 84% at 370 nm. (Figure 9b,c, and entry 1 in **Table 1**). In addition, the effect of stirring speed and direction on photoactivity (being decisive factors in determining the piezopotential) was also discussed, and the fast speed and vertical flow direction of water toward the photoanode surface can efficiently accelerate the photoelectrocatalytic reaction rate.

Besides, some other ZnO-based junctions such as Si/V-doped ZnO nanosheet,[61] TiO_2/ZnO nanowire,[46] n-ZnO/p-SnS core–shell nanostructure,[62] n-ZnO nanoarrays/p-Cu_2O,[49] also perform significantly enhanced water-splitting activities in the presence of polarization charges. Principally, the performance variation in photo(electro)catalytic water splitting is attributed to the changed barrier height at the semiconductor interface, which is resulted from the piezopotential and built-in electric field.[37] In-depth analysis of the relationship between piezopotential and barrier height has been investigated. Through both experiments and calculation results, Wang's group find that the changed barrier height ($\Delta\varphi_{pz}$) at ZnO/ITO interface exhibits a liner relationship with the applied strain, with a barrier height decrease of ≈1.5 mV per 0.1% strain. By regarding the model of piezoelectric ZnO film between ITO and electrolyte, the nonideal remnant polarization can induce a linear potential distribution in ZnO and an exponential potential decay in the screening regions between two electrodes (Figure 9d,f, entry 4 in Table 1).[55] Other approaches including alternative current (AC) impedance spectroscopy may also be effective in distinguishing the piezotronic and piezoresistive effects in a strained Cu/ZnO junction, which clarifies the dominant role of piezotronic effect.[63]

Pollutant Degradation: Polarized charge and piezopotential induced by strain are helpful in engineering the band structure at heterojunction interfaces and accelerating the separation of photoinduced electron–hole pairs, therefore achieving a synergetic effect between photocatalysis and piezocatalysis. Ultrasonication and stirring are common approaches to induce piezopotential in suspending photocatalytic systems. One major application is the removal and degradation of pollutant (such as methylene blue (MB), methyl orange (MO), natural red, rhodamine B, and crude oil) in aqueous solution by ZnO.[56,57,64,65] Recently, Liu et al. reported the piezoelectric process enhanced ZnO nanorods for acid orange 7 (AO7) dye decomposition under ultrasonic vibration.[37] And the activity can be further enhanced by loading cocatalysts and some plasmonic metals (such as Au, Ag).[52,66,67] Several composites by combining ZnO with another narrow bandgap semiconductor like Ag_2S and p-Si have been constructed to modulate the transport property of the photoinduced carriers and extend the light response to visible-light range, which are significant in future research.[66,68]

The structure modulation of ZnO like nanoarrays, nanotetrapods, core–shell composites and immobilization or loading ZnO onto certain flexible or 3D porous supports are also effective ways.[67,69,70] For example, Wang and Li et al. reported the superior performances of ZnO/C nanocomposite and ZnO/Ni foam in photocatalytic degradation of methylene blue,[53,71] and the intensity and frequency of the built-in piezoelectric field with ultrasonic assistance are usually proportional to the ZnO degradation efficiency.[57] For ZnO nanorods vertically grown on 3D Ni foam, when the solution is stirred by magnetic

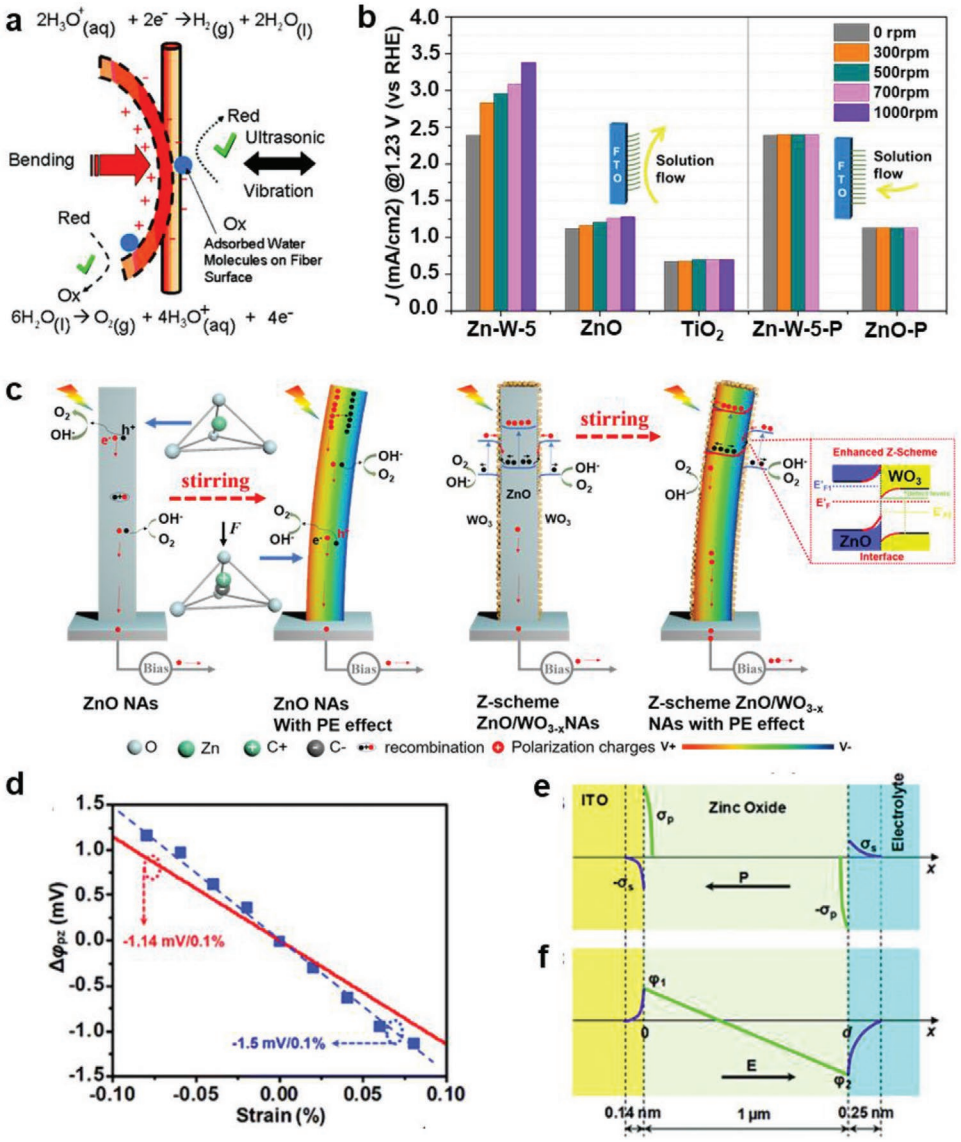

Figure 9. a) Schematic illustration of H_2 and O_2 production by deforming a ZnO fiber in water via oxidation–reduction reactions. Reproduced with permission.[60] Copyright 2010, American Chemical Society. b) Comparison of photocurrents (at 1.23 V vs RHE) of Z-scheme ZnO/WO_{3-x} photoanodes under different stirring rates and strain directions. The flow directions are two types: vertical flow (for Zn-W-5, ZnO and TiO_2) and parallel flow of nanorod arrays (for Zn-W-5-P and ZnO-P). c) Schematic diagram of the polarization process of ZnO, and the reaction process and band structure of Zn-W samples. Reproduced with permission.[26] Copyright 2019, Elsevier. d) Barrier height change ($\Delta\varphi_{pz}$) as a function of strain: $\Delta\varphi_{pz}$ determined from experimental results (blue squares) gives a barrier height change of ≈1.5 mV per 0.1% applied strain. Calculated relationship (red line) shows a smaller changing rate (–1.14 mV per 0.1% applied strain) possibly due to the deviation of screen lengths estimation. Schematic diagrams of the charge density distributions e) and potential profiles f) in ZnO, ITO, and electrolyte solution. Reproduced with permission.[55] Copyright 2011, American Chemical Society.

stirring, fluid eddies are produced in the macroporous structure and the ZnO nanorod are deformed to generate piezoelectric field, leading to an five times enhanced efficiency (entry 15 in Table 1).[53]

Moreover, the ZnO-based heterojunctions with tunable internal stress have also been constructed for the spontaneous piezo-induced effect, through cooling ZnO/TiO_2 heterojunction from high temperature to room temperature with different decreasing rates (based on the mismatched thermal expansion coefficient of the two materials). Accordingly, the photocatalytic degradation performances of methyl orange and methylene blue were improved up to 20% by the induced residual strain in the hybrid structure, with the degradation efficiency of MB reaching 100% in 60 min (**Figure 10**a–c, entry 16 in Table 1).[40]

The extension of optical response from ultraviolet to visible light is also important in promoting the solar-conversion efficiency. For example, a ultrasonication-assisted piezocatalytic type-II CuS/ZnO nanowires exhibit superior performance in degrading methylene blue under solar light irradiation.[50] As shown in Figure 10d,e, the photoinduced

Table 1. Summary of applications of ZnO-based piezoelectric materials.

No.	Catalysts	Reaction conditions	Applications	Activities	Enhancements[a)]	Ref.
			Water splitting			
1	ZnO-WO_{3-x} nanorods	300 W Xe lamp, stirring, 1 mol L^{-1} Na_2SO_4	PEC[b)] water splitting	3.38 mA cm^{-2} at 1.23 V vs RHE	1.42	[26]
2	$Ni(OH)_2$-ZnO	150 W Xe lamp, external strain, 1 mol L^{-1} Na_2SO_3	PEC water splitting	0.74 mA cm^{-2} at 1.5 V vs SCE	1.85	[54]
3	$Ni(OH)_2$-ZnO	150 W Xe lamp, external strain, DI water	PEC water splitting	0.268 mA cm^{-2} at 1.0 V vs SCE	≈1.08	[54]
4	ZnO	Xe lamp, external strain, 0.5 mol L^{-1} K_2SO_4	PEC water splitting	0.60 mA cm^{-2} at 1.5 V vs SCE	≈1.11	[55]
5	TiO_2/ZnO nanowires	300 W Xe lamp, ultrasonic (piezocatalytic), 20 vol% methanol	photocatalytic H_2 production	3.05 µmol g^{-1} L^{-1}	1.54	[46]
			Pollutant degradation			
6	Immobilized ZnO nanowires	9 W florescent tubes (λ = 375 nm), ultrasonic (piezocatalytic), 10 mmol L^{-1}	MB degradation	k = 0.0091 min^{-1} ≈80% in 180 min	1.20	[64]
7	ZnO nanorods	UV, shake, 10 mg L^{-1}	MO degradation	k = 0.0025 min^{-1} ≈70% in 120 min	3.01	[57]
8	ZnO nanowires	50 W Hg lamp, ultrasonic (piezocatalytic), 5 mg L^{-1}	MB degradation	96% in 120 min	≈1.59	[56]
9	ZnO nanorods	UV light (λ = 365 nm), ultrasonic (piezocatalytic), 10 mg L^{-1}	AO7 degradation	k = 0.01726 min^{-1} ≈80.8% in 100 min	1.86	[37]
10	Ag_2S/ZnO	simulated sunlight, ultrasonic (piezocatalytic), 1 mg L^{-1}	MB degradation	100% in 2 h	>1.21	[66]
11	Au/ZnO	300 W Xe lamp (λ = 350 nm), ultrasonic (piezocatalytic), 10 ppm	RhB degradation	k = 0.0759 min^{-1} ≈100% in 20 min	2.61	[52]
12	Ag/ZnO nanowires	UV light (λ = 254 nm), bent, 50 mmol L^{-1}	MB degradation	k = 0.59 µmol min^{-1} ≈100% in 135 min	1.40	[58]
13	Ag/ZnO	300 W Xe lamp, ultrasonic (piezocatalytic), 5 mg L^{-1}	MO degradation	100% in 25 min	>1.15	[67]
14	ZnO/C	300 W Xe lamp, ultrasonic (piezocatalytic), 0.04 mmol L^{-1}	MB degradation	K ≈ 0.015 min^{-1} 100% in 15 min	≈1.67	[71]
15	ZnO/3D Ni foam	100 W Xe lamp (λ = 365 nm), stirring, 5 mg L^{-1}	MB degradation	k = 0.026 min^{-1}	≈5.00	[53]
16	ZnO/TiO_2 nanoplatelets	500 W Hg lamp, thermal stress, MO 20 mg L^{-1}, MB 5 mg L^{-1}	MB/MO degradation	100% of MB in 60 min, 99% of MO in 90 min	–	[40]
17	ZnO@TiO_2	100 W Hg lamp (λ = 365 nm), ultrasonic (piezocatalytic), 10 mg L^{-1}	MO degradation	≈90% in 2 h	≈1.64	[69]
18	CuS/ZnO	500 W Xe lamp, ultrasonic (piezocatalytic), 5 mg L^{-1}	MB degradation	k = 0.18236 min^{-1} 99% in 20 min	3.93	[50]
19	Ag_2O/tetrapod-ZnO	50 W UV light, ultrasonic (piezocatalytic)	MB degradation	99% in 2 min	>1.31	[51]
20	ZnO nanorods	UV–vis light, ultrasonic (piezocatalytic)	photocatalytic CO_2 reduction	16.1 µL g^{-1} h^{-1} (CO), 1.58 µL g^{-1} h^{-1} (CH_4)	1.43/1.95	[72]

[a)]Enhancement refers to the ratio of piezo-phototronic activity/photocatalytic activity for a certain catalyst; [b)]PEC: photoelectrocatalytic; [c)]MB: methylene blue, MO: methyl orange, RhB: rhodamine B, AO7: acid orange 7.

electrons in CB of CuS migrate into ZnO CB while the photoinduced holes transfer in opposite direction. Importantly, the piezoelectric field created by ZnO nanowires can further significantly separate the charges and lower the recombination rate. Attributed to the coupling of the built-in electric field of heterostructures and the piezoelectric field, the reaction kinetics for CuS/ZnO nanowires under both solar and ultrasonic irradiation is 3.9 times faster than that under only solar irradiation, and the degradation efficiency of MB is 99% in 20 min (Figure 10f, entry 18 in Table 1). The reaction mechanism for the piezo-photocatalytic degradation can be expressed as follows

$$\text{photocatalyst} + h\nu \rightarrow \text{CuS}\left(\text{h}^+\right) + \text{ZnO}(\text{e}^-) \quad (14)$$

$$\text{OH}^- + \text{h}^+ \rightarrow \bullet\text{OH} \quad (15)$$

$$\text{O}_2 + \text{e}^- \rightarrow \bullet\text{O}_2^- \quad (16)$$

$$\text{H}^+ + \bullet\text{O}_2^- \rightarrow \text{HO}_2\bullet \quad (17)$$

$$2\text{HO}_2\bullet \rightarrow \text{H}_2\text{O}_2 + \text{O}_2 \quad (18)$$

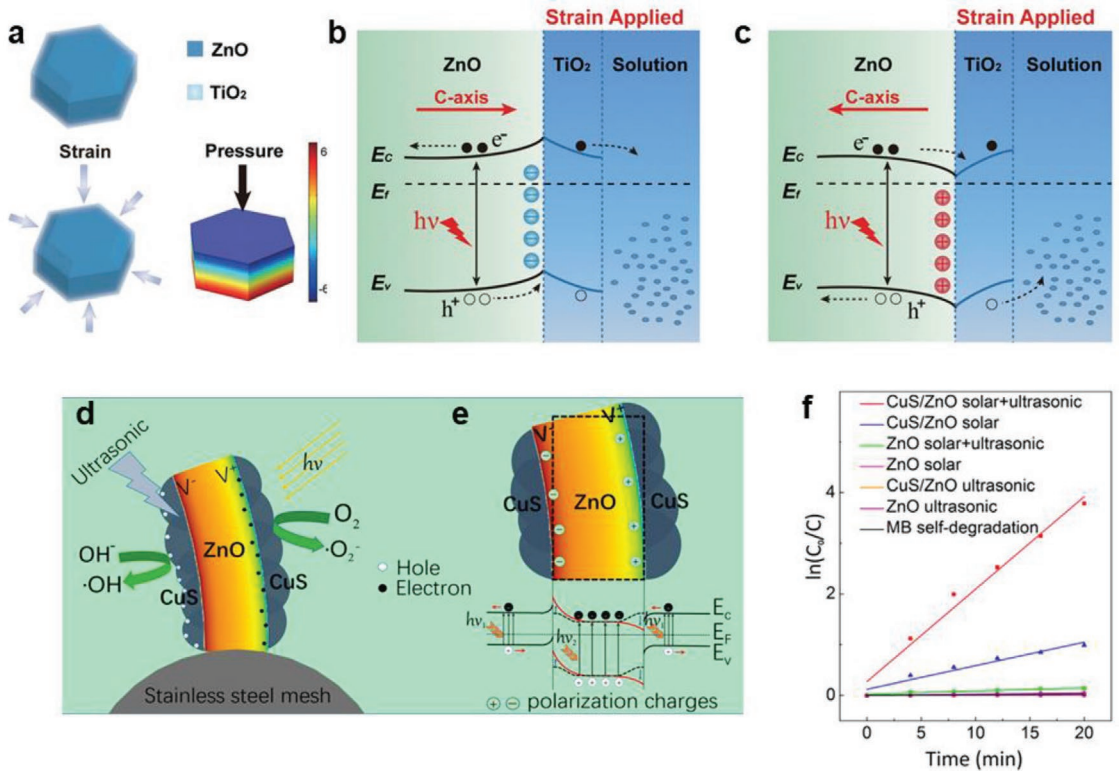

Figure 10. a) Schematic illustration of ZnO/TiO_2 hybrids without (top) and with strain (bottom left). Piezopotential distributions in a ZnO nanoplatelet (hexagonal edge: 2 µm, height: 1.5 µm) under an axial pressure of 10 MPa, simulated by a finite-element analysis method (bottom right). b,c) Band diagrams of strain (tensile or compressive) applied ZnO/TiO_2 heterojunction (along *c*-axis of ZnO). Reproduced with permission.[40] Copyright 2016, American Chemical Society. d) Schematic illustration of the piezo-enhanced photocatalytic process of CuS/ZnO nanowires on stainless steel mesh under both solar irradiation and piezocatalytic (ultrasonic) treatment. e) Schematic illustration of the energy band bending diagram of CuS/ZnO heterostructure under both solar irradiation and piezocatalytic (ultrasonic) treatment. f) Photocatalytic degradation kinetic of methylene blue over ZnO and CuS/ZnO under different reaction conditions (including self-degradation of methylene blue). Reproduced with permission.[50] Copyright 2016, American Chemical Society.

$$\bullet O_2^- + H_2O_2 \rightarrow \bullet OH + OH^- + O_2 \quad (19)$$

$$\bullet OH + \text{dye} \rightarrow \text{inorganic ions} + H_2O + CO_2\,(HCOOH) \quad (20)$$

In addition to water splitting and degradation, the denser electrons induced by ultrasonic irradiation can also help to improve the performance of other photocatalytic reactions like CO_2 reduction (entry 20 in Table 1).[72]

Summaries of typical ZnO-based catalysts (including the above-mentioned catalysts) on piezo-promoted photo(electro) catalytic processes are listed in Table 1.

4.1.2. Metal Niobates

Several niobates ($KNbO_3$, $NaNbO_3$, $AgNbO_3$ with general formula of ABO_3, where A is a metal, B is second metal Nb, and O is oxygen, space group A*mm*2, **Figure 11**a) are typical ferroelectric perovskites with the advantages of nontoxicity, cost-effectiveness, and high photostability. Niobates are often used as frequency-converting materials, optical waveguides and holographic storage media.[73] Taking $KNbO_3$ as an example, it goes through a series of phase transitions from rhombohedral, orthorhombic (start at about −10 °C), tetragonal (at about 225 °C) to cubic (at about 437 °C). In orthorhombic phase (point group *mm*2) at room temperature, ferroelectric polarization is nominally constrained to one of the symmetry-equivalent face-diagonals of the perovskite pseudocube, yielding a total of 12 possible orientations of the ferroelectric domains.[74] Meanwhile, these materials have outstanding photocatalytic properties, thus increasing interests on metal niobates have been intensified for their piezo-induced photo(electro)catalytic applications.

Water Splitting: $KNbO_3$ and $NaNbO_3$ are promising candidates for photocatalytic water oxidation. Yu et al. reported $KNbO_3$ with optimal poling configuration as photoanode for water splitting, which exhibits significant activity enhancement.[41] Singh and Khare synthesized $NaNbO_3$ to enhance the efficiency of photoelectrochemical water splitting.[75] Notably, $NaNbO_3$/ITO (with polyethylene terephthalate as substrate) was polarized by applying an external electric field. They find that the built-in piezopotential along with a band alignment can be induced under periodic mechanical strain, which enhances the separation of photoinduced carriers and the performance of water splitting. Compared with $NaNbO_3$ photoanode without external strain, the photocurrent density of the one under piezopotential induced by ultrasonic vibrations increases from 0.78 to 1.02 mA cm^{-2}, and the IPCE efficiency is enhanced by 8% (Figure 11b,c, entry 1

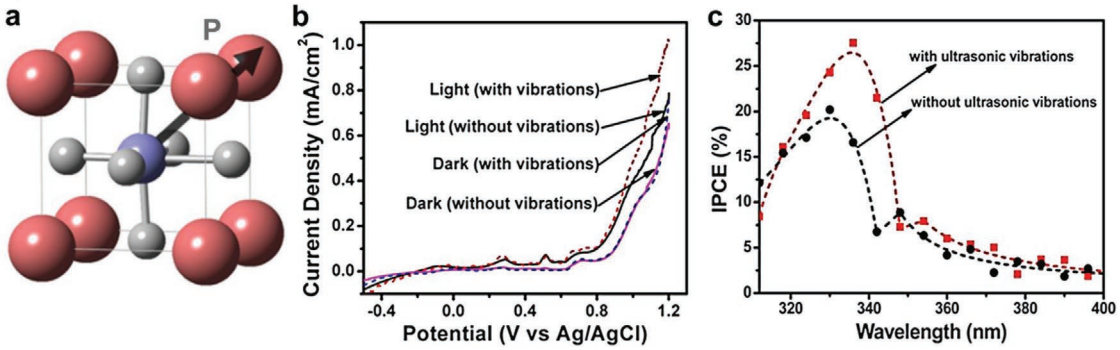

Figure 11. a) Typical structure of crystal structure of niobates. Red, purple, and gray spheres represent the metal ions (K, Na), Nb, and O atoms, respectively. The black arrow indicates one of the possible directions of the electric polarization P. Reproduced with permission.[41] Copyright 2019, Elsevier. b) Current-potential curves and c) IPCE efficiency of $NaNbO_3$ photoanodes. Reproduced with permission.[75] Copyright 2017, Elsevier.

in **Table 2**). After that, by introducing poly(vinylidene fluoride)/Cu as new substrates instead of ITO, the water oxidation performance can be further promoted (entry 2 in Table 2).[76]

Moreover, $KNbO_3$ has also been reported as a photocatalyst for water reduction (H_2 evolution).[77,78] For example, Jia et al. designed a novel $MoS_2/KNbO_3$ photocatalyst via a simple

Table 2. Summary of applications of niobates, CdS, $BiFeO_3$ and other 2D-based piezoelectric materials.

No.	Catalysts	Reaction conditions	Applications	Activities	Enhancements	Ref.
			Water splitting			
1	$NaNbO_3$	tungsten halogen lamp, ultrasonic (piezocatalytic), 1 mol L^{-1} Na_2SO_4	PEC water splitting	1.02 mA cm^{-2} at 1.2 V vs Ag/Cl	1.31	[75]
2	PVDF/Cu/PVDF–$NaNbO_3$	simulated sunlight, poling and ultrasonic (piezocatalytic), 0.5 mol L^{-1} NaOH	PEC water splitting	≈1.73 mA cm^{-2} at 1 V vs Ag/Cl	2.40	[76]
3	$MoS_2/KNbO_3$	300 W Xe lamp, ultrasonic (piezocatalytic), 15 vol% triethanolamine	photocatalytic H_2 production	96 μmol g^{-1} h^{-1}	2.00	[78]
4	CdS	300 W Xe lamp, disturbances, 10 vol% lactic acid	photocatalytic H_2 production	10.4 mmol g^{-1} h^{-1}	4.00	[47]
5	CdS	300 W Xe lamp, ultrasonic (piezocatalytic)	photocatalytic H_2 production	60 μL h^{-1}	1.50	[81]
6	$BiFeO_3$	300 W Xe lamp, poled, 0.1 mol L^{-1} KCl	PEC water splitting	10 μA cm^{-2} at 0 V vs Ag/Cl	–	[83]
7	$ZnSnO_3$	150 W Xe lamp, ultrasonic (piezocatalytic)	photocatalytic H_2 production	6000 μmol g^{-1} in 7 h	–	[36]
			Pollutant degradation			
8	$KNbO_3$ nanosheets	300 W Xe lamp, ultrasonic (piezocatalytic), 10 mg L^{-1}	RhB degradation	$k \approx 22.8$ min^{-1} 92.6% in 120 min	≈3.6	[41]
9	$KNbO_3$ nanocube	300 W Xe lamp, ultrasonic (piezocatalytic), 10 mg L^{-1}	RhB degradation	$k \approx 16.0$ min^{-1} 85% in 120 min	≈1.18	[41]
10	orthorhombic $KNbO_3$	UV light, poling, 0.16 mmol L^{-1}	RhB degradation	$k = 0.042$ min^{-1} 60% in 210 min	–	[31]
11	monoclinic $KNbO_3$	UV light, poling, 0.16 mmol L^{-1}	RhB degradation	$k = 0.020$ min^{-1} 35% in 210 min	–	[31]
12	$NaNbO_3$	tungsten halogen lamp, ultrasonic (piezocatalytic), 0.04 mmol L^{-1}	MB degradation	$k \approx 0.01$ min^{-1} 78% in 180 min	2.15	[75]
13	$KNbO_3/MoS_2$	300 W Xe lamp, ultrasonic (piezocatalytic), 10 mg L^{-1}	RhB degradation	$k = 0.037$ min^{-1} 95% in 60 min	3.70	[78]
14	$BiFeO_3/TiO_2$	300 W Xe lamp, ultrasonic (piezocatalytic), 10 ppm	methyl violet degradation	$k = 0.024$ min^{-1} 100% in 120 min	3.88	[84]
15	$ZnSnO_3$	150 W Xe lamp, ultrasonic (piezocatalytic)	RhB degradation	$k \approx 108$ s^{-1} 92% in 1 h	≈1.44	[36]
16	Au/MoS_2	near-infrared light, vibration	*E. coli* disinfection	99.9999% in 15 min	3.00	[96]

hydrothermal method, which exhibits effective photocatalytic H_2 production under Xe lamp illumination. And the photocatalytic activity is two times improved by utilizing ultrasonic energy to generate internal piezoelectric field for charge transfer (entry 3 in Table 2).[78]

Pollutant Degradation: The strong oxidizing potential of photoinduced holes from metal niobates enables its high activity in degradation, which can be further promoted by piezoelectric effect. For example, $NaNbO_3$ emerges high performance in decomposing rhodamine B dye through the piezo-catalytic effect.[79] Yu et al. further reveal that the piezo-polarization of $KNbO_3$ nanosheets can be efficiently tuned by changing its poling configuration, which achieves 92.6% degradation of RhB in 120 min with a reaction constant of $k \approx 22.8$ min^{-1} (entries 8,9 in Table 2).[41] With the going deep of research work, the understanding of structure–function correlations in such perovskite-based semiconductors becomes a central theme, and increasing attention has been paid on the direct visualization of surface active sites, measurement of local atomic displacements at an accuracy of several picometers, and quantification of piezo-polarization through theoretical calculations.[31]

Summaries of typical niobate-based materials (including the above-mentioned catalysts) on piezo-promoted photocatalytic and photoelectrocatalytic processes are listed in Table 2.

4.1.3. Cadmium Sulfide (CdS)

CdS is one of the earliest discovered piezoelectric components, and widely adopted in photocatalytic hydrogen generation, pollutant degradation and photoelectrocatalytic water splitting. Therefore, CdS semiconductor that combine piezoelectric and visible-light photocatalytic properties show great potentials in piezo-phototronics.[80] Zhao et al. report visible-light-driven H_2 evolution from pure water by bare CdS without any cocatalysts, through conducting a piezoelectric photocatalysis strategy. The external strain (ultrasonic) induced piezoelectric field in CdS alters the separation of photoinduced charges, and the H_2 production rate obviously varies with the ultrasonic frequency after normalizing by sound intensities. Optimally, under coupling field with the maximum deformation at the resonance frequency of CdS nanorods (27 kHz), a high H_2 production rate of 20 μL h^{-1} is achieved. This signifies that the synergy for photoacoustic H_2 evolution follows a second mechanism in which ultrasound-induced piezoelectric field promotes the separation of photoinduced charges (**Figure 12**).[81] In another work, when applying magnetic stirring to induce piezoelectric effect, the photocatalytic H_2 evolution rate by CdS reaches 10.4 mmol g^{-1} h^{-1}, increasing by nearly four times of bare photocatalyst, which can respond to the self-powered energy from mechanical disturbances for piezoelectric-enhanced photocatalysis.[47] Similarly, Zhou et al. has demonstrated the piezotronic effect in vertically aligned CdSe nanowire arrays,[82] and indicated that CdSe is a promising candidate in piezo-phototronics. With the change of strain of 0.12%, a current decreased from 84 to 17 pA at 2 V bias. And the Schottky barrier between Pt and CdSe is found to be elevated by applying external force/stress on CdSe nanowire.

4.1.4. Bismuth Ferrite ($BiFeO_3$)

$BiFeO_3$ is also a typical ferroelectric material with a bandgap of 2.2 eV. Cao et al. reveal that $BiFeO_3$ can be adopted as photoelectrode in form of modifier/$BiFeO_3$/ITO, and the transfer of charges generated either in $BiFeO_3$ or surface modifiers (that can inject excited charges to $BiFeO_3$ such as molecular dyes) is manipulated by the poling pretreatment.[83] Attributed to the prominent ferroelectric properties, the photocurrent could be switched from 0 to 10 mA cm^{-2} with the change of poling bias.

Another typical example is the nanocomposite construction like $BiFeO_3/TiO_2$, and the introduction of piezoelectric polarization can enhance its photodegradation activity of dye molecules by 4.3 times (**Figure 13**a,b).[84] In detail, when polarization charge is created by ultrasonic wave (piezocatalytic), the electrons and holes are polarized along its spontaneous polarization axis. The band edge thereby becomes steeper, and the charge transfer direction can be modulated by polarization direction (Figure 13c,d). Therefore, the piezopotential induced by external mechanical force generates robust built-in potential from the band alignment at the junction interface, which significantly enhances the separation of photoinduced charge pairs.

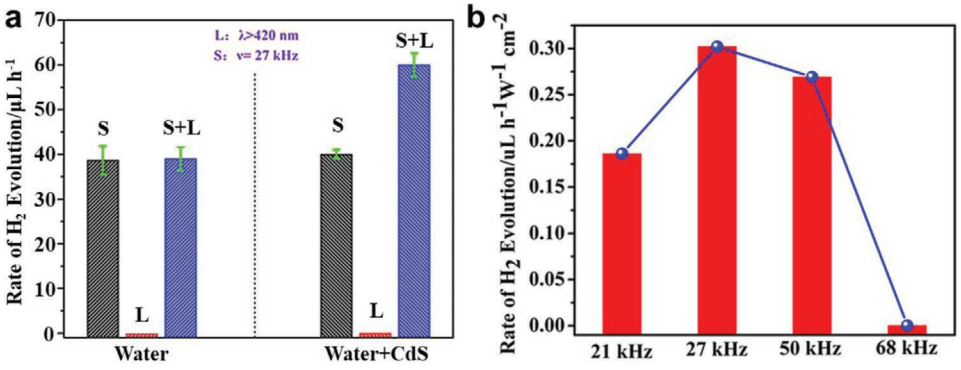

Figure 12. a) Rates of hydrogen production from water at different conditions (in water with/without CdS), L refers to visible-light irradiation, S refers to ultrasonic vibration, respectively. b) The frequency-dependent change of hydrogen evolution rate normalized by acoustic intensity. Reproduced with permission.[81] Copyright 2018, Wiley-VCH.

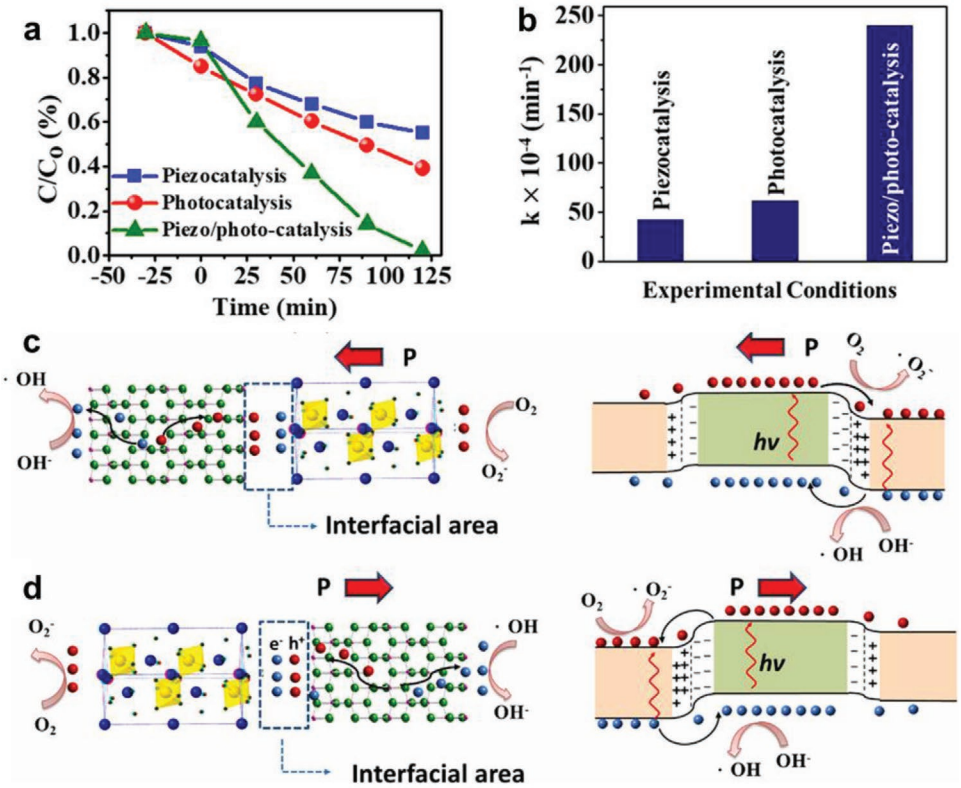

Figure 13. a) High-resolution TEM images of $BiFeO_3/TiO_2$ heterojunction. b) Comparison of degradation activities over the $BiFeO_3/TiO_2$ under piezo-catalysis, photocatalysis, and piezo-phototronic catalysis. c,d) Piezo-phototronic processes of $BiFeO_3/TiO_2$ with the different direction of polarization. Reproduced with permission.[84] Copyright 2019, Elsevier.

4.1.5. Other Materials

Besides of the above-mentioned materials, other materials like $SrBi_4Ti_4O_{15}$, $ZnSnO_3$, and BiOCl have also been utilized for piezo-photocatalysis.

$SrBi_4Ti_4O_{15}$: $SrBi_4Ti_4O_{15}$ is a type of ferroelectric and piezotronic, layered bismuth-based and perovskite-structured crystal, which shows great potential in photocatalysis. In 2018, Tu et al. reported that ferroelectric $SrBi_4Ti_4O_{15}$ can be a robust photocatalyst for CO_2 reduction, which achieved a notable photocatalytic CH_4 evolution activity of 19.8 μmol g^{-1} h^{-1} and an apparent quantum efficiency of 1.33% at 365 nm. Ferroelectric hysteresis loop, piezo-response force microscopy (PFM) and theoretical calculations demonstrated that a strong ferroelectric spontaneous polarization distributes along the [100] direction of $SrBi_4Ti_4O_{15}$, and both electrons and holes showed the smallest effective mass, facilitating charge transfer.[85]

$ZnSnO_3$: $ZnSnO_3$ possesses various features of interest, and has been reported for gas sensors, nanogenerators and photocatalysis. According to theoretical calculation, LN-type $ZnSnO_3$ (space group *R3c*) is very promising for piezoelectric application. Although $ZnSnO_3$ is reported as a metastable material, its hydrothermal synthesis can offer an ideal platform for fabricating stabilized $ZnSnO_3$ phase.[86] $ZnSnO_3$ was recently recognized as a potential piezo-photocatalyst, and its piezoelectricity was utilized to enhance photocatalysis (like the degradation of methylene blue) under ultrasonic vibration.[86,87] Wang et al. find that when ultrasonic vibration and external force were applied simultaneously, the degradation activity of methylene blue was 3.7 times enhanced than bare photocatalysis.[86] However, $ZnSnO_3$ suffers from a large bandgap of nearly 3.8 eV (that only a portion of ultraviolet light can be absorbed), thus approaches to extending its light-absorption range are necessary. Recently, Wang et al. first applied the $ZnSnO_3$ nanowires (space group *R3c*) for the piezo-photocatalytic H_2 evolution. Through introducing oxygen vacancies by thermal annealing in hydrogen environment, the bandgap of $ZnSnO_3$ is reduced to extend light response. Meanwhile the mechanical-force-induced polarization enhances the charge separation. Consequently, the optimized $ZnSnO_3$ catalysts achieved a degradation efficiency of ≈ 92% for dye molecules while the HER reached about 6000 μmol g^{-1} in 7 h.[36] Their work provides an effective strategy for modulating $ZnSnO_3$ in piezo-phototronic reaction.

Bismuth Oxychloride (BiOCl): As a typical photocatalyst, BiOCl also shows piezo-catalytic activity for oxygen reduction reaction to produce H_2O_2. The piezoelectric response of BiOCl was directly confirmed by PFM, and the built-in electric field induced by piezopotential (under ultrasonic wave) can efficiently drive electrons to react with O_2 and H_2O, then forming H_2O_2 with the rate of 28 μmol h^{-1}.[88] Therefore, the integration of piezo-catalytic approach with photocatalysis is expected as a promising approach to further boost the reaction efficiency.

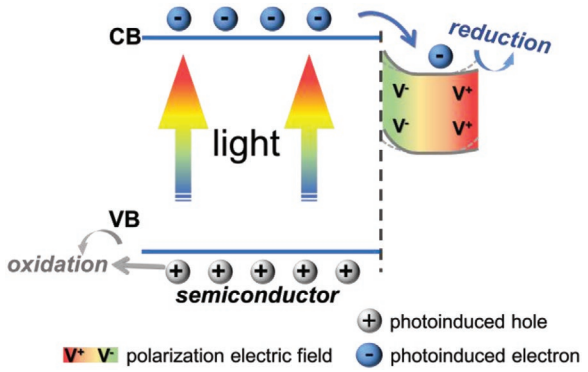

Figure 14. Schematic diagram of the mechanism of material with synergetic piezoelectric and conductive properties. The dashed line represents the initial band edge without strain while the solid line represents the band edge under strain.

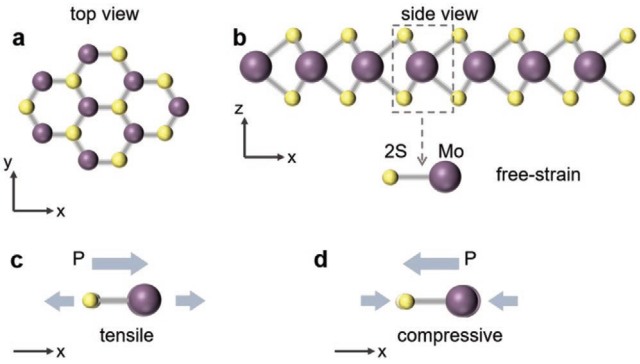

Figure 15. a) Top and b) side views of the atomic structure of MoS_2 and Mo-2S dipoles in free-strain state. *X*-axis c) tensile stain and d) compressive stain induced piezo-polarization of Mo-2S dipoles, P and black arrow indicate the possible directions of electric polarization. Reproduced with permission.[39] Copyright 2016, Wiley-VCH.

4.2. Material with Synergetic Piezoelectric and Conductive (without Photocatalytic) Properties

The category of piezoelectric materials with conductive properties possess great advantages in photo(electro)catalysis, which are capable of generating piezopotential and simultaneous acting as cocatalysts. Thereby both charge migration and redox kinetics can be promoted. They cannot act as photocatalysts (generating effective charges for redox reaction) individually. The mechanism is illustrated in **Figure 14**.

4.2.1. 2D Material—Molybdenum Disulfide (MoS_2)

2D MoS_2 is thermodynamically stable and can be easily synthesized with great potential for optoelectronic and other applications.[89] As reported, MoS_2 possesses a suitable free energy for H_2 absorption ($\Delta G_H \approx 0.08$ eV), which are considered to be the most promising non-noble metal alternative to Pt. Therefore, MoS_2 is now widely adopted as electrocatalysts and photocatalytic cocatalysts. MoS_2 is composed of the "S–Mo–S" intercalating layers by van der Waals force. The anisotropic structure and weak interlayer force imply the possibility of breaking interlayer force and exfoliating bulk structures to create more edge sites and expose abundant active sites, and consequently to enhance the catalytic performances.[90]

Recently, low-dimensional MoS_2 has been regarded as an alternative choice for piezo-catalysis.[78,91,92] As shown in **Figure 15**, the D_{3h} point group symmetric MoS_2 (one Mo layer in two S layers) exhibits identical Mo−S bond length of 2.42 Å. If the Mo-2S dipoles are stretched, a spontaneous polarization points from S to Mo along with armchair direction (+*x* direction) is thereby created. And the induced electric field is propagated and aligned with the −*x* direction. In contrast, when a compressive strain is applied, an opposite polarization field will be generated. The electric field induced by spontaneous polarization is parallel to the direction of external force, and the electric field serves as an efficient driving force for unidirectional charge separation. Basically, the piezoelectric effect of MoS_2 increases with the decline of its layer number and reaches maximum in monolayer since there is significant interaction in the interface of MoS_2 hybrid.[39,91]

In 2016, Wu et al. discovered the piezo-catalytic effect of single- and few-layer MoS_2 for the first time, which exhibited an ultrahigh degradation activity by introducing the ultrasonic wave in dark condition.[39] This is able to open up a prodigious possibility for the future catalytic applications of MoS_2. Another work also from Wu et al. reported that the generation of hydroxyl radicals in waste water can be promoted by piezoelectric spontaneous polarization around the single- and odd number of MoS_2 layers through applying mechanical force, which lead to a rapid dye degradation kinetics. Moreover, the intensity of H_2 generation was also increased with the concentration of MoS_2.[93] This work verifies the feasibility of both photocatalytic degradation and hydrogen evolution by utilizing the piezoelectricity of MoS_2 in dark environment. It can be therefore speculated that MoS_2 is a very promising candidate for photocatalytic and photoelectrocatalytic applications.

However, pure MoS_2 still suffers from low charge-separation efficiency and unsatisfying stability under light irradiation. Approaches including morphological modulation, cocatalysts loading, and heterojunction construction can be effective in further enhancing its performance.[94] Liu et al. designed TiO_2–MoS_2 hybrids toward piezo-enhanced degradation of rhodamine B, and the decoloration efficiency reaches 84% in 25 min. Hence, the piezo-catalytic property of MoS_2 is first proved to be survivable in hybrid structure.[93,95] Some researchers also demonstrated that MoS_2 can catalyze the production of reactive oxygen species to inactivate *Escherichia coli* bacteria up to 99.999% via piezo-enhanced photocatalysis.[96] These works strongly demonstrate that the hybridization of piezoelectric and photocatalytic effects will lead to a performance much superior to that obtained with the individual ones.

4.2.2. Other 2D Transition Metal Dichalcogenides

2D transition metal dichalcogenides (TMDs) like WS_2, WSe_2, and $MoSe_2$ with similar electronic or structural properties have also been recently adopted in piezo-photocatalysis.[92,97,98] The electric properties of these TMDs are similar to those of MoS_2.

And most of the monolayer TMDs are intrinsically piezoelectric due to the lack of structural central symmetry, which offers them a new degree of freedom to interact with external mechanical stimuli. For instance, Wu et al. recently reported single and few layers WS_2 nanoflower embedded in polydimethylsiloxane (with its piezoelectric property detected by PFM and tunneling atomic force microscopy, TUNA) for the degradation of rhodamine B and disinfection of *E. coli* in dark environment.[97] Thus, it can be seen that such TMDs are promising for photo(electro) catalysis especially when combining with appropriate visible-response semiconductors.

4.2.3. Niobium Nitride

TMDs with properties similar to MoS_2 are often related to the orbital occupation or d-electron configuration (d^2) of the transition metal atom. This configuration (d^2) is also possibly existed in compounds with other 4d cations including Nb^{3+}, Zr^{2+}, and Tc^{5+}. Although transition metal dichalcogenides have exhibited superior in piezo-photonics, it suffers a major drawback of unstable phase transfer (from 1T to 1H) upon high temperature, thereby vanishing its intrinsic piezo-property.[91,99] Toward this, transition metal nitride like NbN compounds, which have similar properties to MoS_2 but more robust against interpolymeric transitions, gradually arouse attention of researchers. Although no experimental research is reported yet, first-principle calculations have predicted the great potential of NbN in piezo-enhanced photocatalytic processes.[100]

4.3. Coupling of Piezoelectric Material (without Photocatalytic Property) and Photocatalyst

With the deepening of research, more and more piezoelectric materials have been demonstrated to be effective in photo(electro)catalysis. Some piezoelectric materials are intrinsically nonconducting or is hardly to be excited with a large bandgap. They are not photocatalysts but can produce piezo charges and generate a built-in electric field. Given the absence of photo-response or conductive properties in crystal structures, the coupling of microcosmic polarization from polar materials with photocatalytic semiconductors can result in a large macroscopic polarization as the driving force for charge transfer and separation, thus benefitting solar conversion efficiency (**Figure 16**). The most widely applied piezoelectric materials are barium titanate and polyvinylidene fluoride (PVDF), with the coupling of typical photocatalysts like TiO_2, plasmonic Al, Ag, Au, Ag_2O, etc.

4.3.1. Barium Titanate

The discovery of photocatalytic property in TiO_2 opens a new chapter in solar energy conversion. Although TiO_2 is generally centrosymmetric without piezotronic properties, several titanites are available in piezo-photonics, among which $BaTiO_3$ is the first polycrystalline ceramic material ever discovered that exhibits ferroelectricity and recently adopted in photocatalysis. As early as in 2009, Liu and Ren have considered the potential

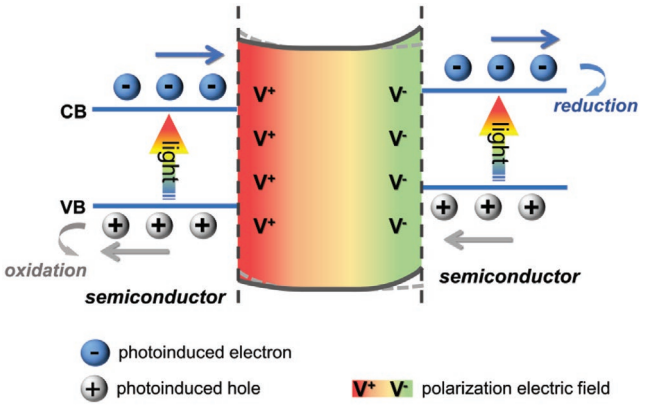

Figure 16. Schematic diagram of the coupling of piezoelectric material and photocatalyst. The dashed line represents the initial band edge without strain while the solid line represents the band edge under strain.

of $BaTiO_3$-based materials for piezoelectric applications.[101] Different from TiO_2, perovskite $BaTiO_3$ undergoes a structural transition at Curie temperature, which leads to the spontaneous ferroelectric polarization from the low-temperature-stable structure of a polar crystal class. In detail, when cooled at ambient pressure, a sequence of first-order phase transitions of $BaTiO_3$ occurs: cubic (space group $Pm3m$) → tetragonal (space group $P4mm$) → orthorhombic (space group $Amm2$) → rhombohedral (space group $R3m$). Such transitions result in a spontaneous polarization directed parallel to the edge (tetragonal) of crystal cell, and its subsequent reorientation along a face diagonal (orthorhombic) and body diagonal (rhombohedral).[102] The piezoelectric property is strongly dependent on the degree of spontaneous polarization.

The first report about ferroelectric $BaTiO_3$-based nanogenerator is presented in 2010, which demonstrated that its performance can be obviously enhanced with the assistance of piezopotential due to periodically bending deformation.[102,103] And recently, $BaTiO_3$ has been recognized as a promising candidate in photocatalysis and photoelectrocatalysis, providing external piezopotential for efficient spatial separation of the photoinduced charges. Other similar materials such as $Na_{0.5}Bi_{0.5}TiO_3$ and perovskite-like $Bi_4Ti_3O_{12}$ are also used in piezo-photonics.[104,105]

Water Splitting: The early report on piezoelectric $BaTiO_3$ microdendrites induced water splitting was promoted by Hong et al.[60] During the recent years, increasing number of $BaTiO_3$-based composites have been fabricated as water splitting catalysts. Some researchers find that the hybridization of piezoelectric $BaTiO_3$ with a secondary metal (including plasmonic Al, Ag, Au) may lead to significantly enhanced photocatalysis. The increased number of redox sites and accelerated separation of plasmonic charges due to the piezopotential of $BaTiO_3$ greatly boost the reaction efficiency. Guo et al. designed Al@$BaTiO_3$ composite on Ti substrate for synergistic piezo-photocatalytic water splitting.[106] Upon magnetic-field-induced strong polarization potential, the synergistic piezo-photocatalysis exhibited almost 50% increase in H_2 production rate, corresponding to 657 μmol h^{-1} cm^{-2} (entry 1 in **Table 3**).

Another approach to further optimize photocatalytic performance is the construction of heterojunctions, including both

Table 3. Summary of applications of metal titanates based piezoelectric materials.

No.	Catalysts	Reaction conditions	Applications	Activities	Enhancements	Ref.
			Water splitting			
1	$Al/BaTiO_3$	simulated sunlight, vibration, 20 vol% methanol	photocatalytic H_2 production	657 μmol cm^{-2} h^{-1}	1.5	[106]
2	$TiO_2/BaTiO_3$	simulated sunlight, poling, 0.5 mol L^{-1} phosphate buffer	PEC water splitting	≈1.36 mA cm^{-2} at 1.23 V vs RHE	–	[107]
3	$TiO_2/BaTiO_3/Ag_2O$	simulated sunlight, poling, 1 mol L^{-1} NaOH	PEC water splitting	1.8 mA cm^{-2} at 0.8 V vs Ag/Cl	1.2	[108]
			Pollutant degradation			
4	Fe^{3+}-doped BaTiO3	150 W Xe lamp, ferroelectric and stirring, 20 mg L^{-1}	MO degradation	k = 0.01346 min^{-1} 75% in 90 min	–	[117]
5	$Al/BaTiO_3$	simulated sunlight, vibration, 0.4 mmol L^{-1}, $NaBH_4$	4-Nitrophenol hydrogenation	100% in 40 min	≈1.5	[106]
6	$Ag–BaTiO_3$	300 W Xe lamp, ultrasonic (piezocatalytic), 0.01 mmol L^{-1}	MB degradation	83% in 75 min	1.2	[111]
7	$Au/BaTiO_3$	300 W Xe lamp, ultrasonic (piezocatalytic), 10 mg L^{-1}	MO degradation	k ≈ 0.0126 min^{-1} 100% in 60 min	≈1.3	[112]
8	$Au/BaTiO_3$	UV light, ferroelectric polarization, 0.02 mmol L^{-1}	RhB degradation	k = 0.05446 min^{-1} ≈95% in 60 min	–	[118]
9	$C_3N_4/BaTiO_3$	visible light, poled, 10 ppm	MO degradation	k ≈ 0.015 min^{-1} ≈95% in 180 min	≈1.8	[119]
10	$ZnO/BaTiO_3$	500 W Xe lamp, ultrasonic (piezocatalytic), 10 mg L^{-1}	RhB degradation	k ≈ 0.118 min^{-1} 97% in 30 min	2.21	[114]
11	$Bi_4Ti_3O_{12}$	300 W Xe lamp, ultrasonic (piezocatalytic), 20 mg L^{-1}	phenol degradation	k ≈ 0.039 min^{-1} 99% in 2 min	>1.3	[105]

binary and ternary composites. The design of $TiO_2/BaTiO_3$ core/shell heterojunction evidences that piezotronic effect holds great promise in improving the performance of photoelectrodes. The design of $TiO_2/BaTiO_3$ core/shell heterojunction evidences that piezotronic effect holds great promise in improving the performance of photoelectrodes. The charge separation efficiency reaches 84.8% at 1.23 V versus RHE, which is 1.67 times of pure TiO_2 (entry 2 in Table 3).[107] Furthermore, Liu et al. reported a ternary $TiO_2/BaTiO_3/Ag_2O$ nanorod array as water splitting photoanode with 2.6 times enhanced activity compared with TiO_2 (**Figure 17**a–c, entry 3 in Table 3). The IPCE is 12% at 500 nm under a bias of 0.5 V, higher than the $TiO_2/BTO/Ag_2O$ without poling.[108] The introduction of a piezoelectric $BaTiO_3$ layer at the interface between p-type Ag_2O and n-type TiO_2 creates a polar-charge-induced electrical field, providing a sustainable driving force that attracts the holes of TiO_2 and the electrons of Ag_2O (Figure 17d).

Pollutant Degradation: $BaTiO_3$ is also a promising candidate in heterojunctions for the photocatalytic degradation of pollutants. Researchers have demonstrated that the introduction of piezopotential from $BaTiO_3$ serves as an effective strategy to enhance the piezocatalytic degradation performance.[33,109] The finite element method (FEM) with aid of COMSOL Multiphysics is adopted in simulating the distribution of piezopotential, and clarifying the relationship between piezopotential and piezocatalytic efficiency (**Figure 18**).[109] In the so-called "piezo-Fenton process," the piezoelectric effect of $BaTiO_3$ nanoparticles could in situ drive the generation of H_2O_2, which is facilely turned into hydroxyl radical, leading to degradation of AO7 pollutants.[110]

Some researchers focused on the interaction of $BaTiO_3$ and metals or electrocatalysts, such as Al, Au, Ag, etc.,[106,111–113] and further clarified the mechanism of the coupling effect between piezotronics and surface plasmonic resonance.[33] For example, Xu et al. reported $Ag–BaTiO_3$ piezo-photocatalysts synthesized by a photochemical reducing approach.[111] The piezoelectric field originated from deformation of $BaTiO_3$ enhances the separation of photoinduced carriers from Ag surface plasma resonance and promotes the formation of oxidizing radicals that could accelerate the degradation of organic dyes. Consequently, the piezoelectric charge and piezopotential on the surfaces of $BaTiO_3$ express an increment of catalytic activity more than 20%. By introducing Au nanoparticles, the visible-light-driven catalytic degradation of methyl orange by $BaTiO_3$ was much enhanced.[112] The cooperation of $BaTiO_3$ with other semiconductors such as $ZnO/BaTiO_3$ heterostructure has also been demonstrated to work well in the degradation of pollutants, which endows a suitable bend alignment formed at the interface to promote charge transfer behavior.[114]

Efforts have also been made to tackle the in-depth role of ferroelectric polarization and the relationship between electric polarization and piezocatalytic activity of $BaTiO_3$. Wu et al.'s study directly indicates that ferroelectric polarization is predominant in enhancing piezocatalytic activity, and demonstrates that the piezopotential makes a big contribution in enhancing charge separation and triggering redox reaction (**Figure 19**a).[115] In another work, Xu et al. used $Au/BaTiO_3$ nanostructures to illustrate the piezo-enhanced plasmonic degradation mechanism.[112] As shown in Figure 19b, when Au is in contact with $BaTiO_3$, a Schottky barrier is formed at the interface due to

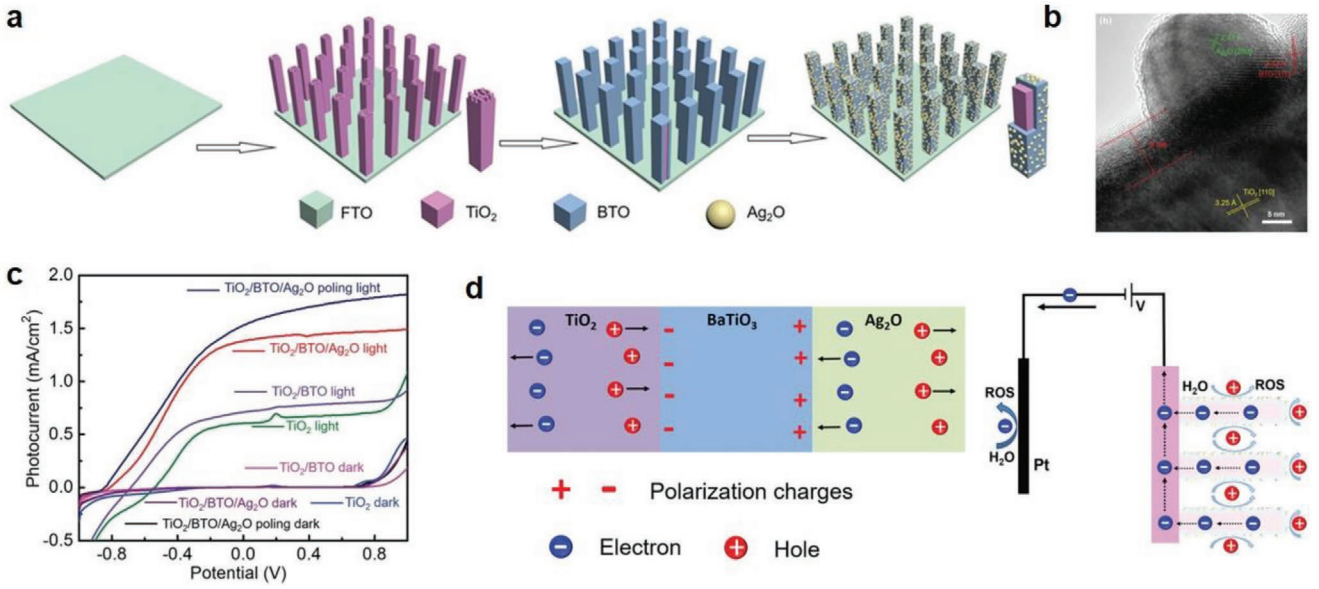

Figure 17. a) Scheme of the fabrication process and b) high resolution transmission electron microscope (TEM) image of TiO_2/BTO($BaTiO_3$)/Ag_2O nanorod arrays. c) Current–voltage curve in dark and under Xe lamp irradiation of different photoanodes. d) Mechanism and reaction pathway for the enhanced photoelectrocatalytic performance for TiO_2/BTO($BaTiO_3$)/Ag_2O. Reproduced with permission.[108] Copyright 2019, Wiley-VCH.

their work function difference (left panel). Under light illumination, the surface electrons of Au exhibit collective oscillations localized surface plasmon resonance (LSPR) and decay into energetic hot electrons. The hot electrons then transfer across the Schottky barrier (Φ_1) to $BaTiO_3$ (middle panel). Additionally, under sonication pressure, the polarization charges of $BaTiO_3$ will induce a built-in piezoelectric field, which further suppress the Schottky barrier energy (Φ_2), retain more excited holes and generate more radicals for oxidation (the right panel). Thus, the photocatalytic efficiency is 1.3 time enhanced than pure

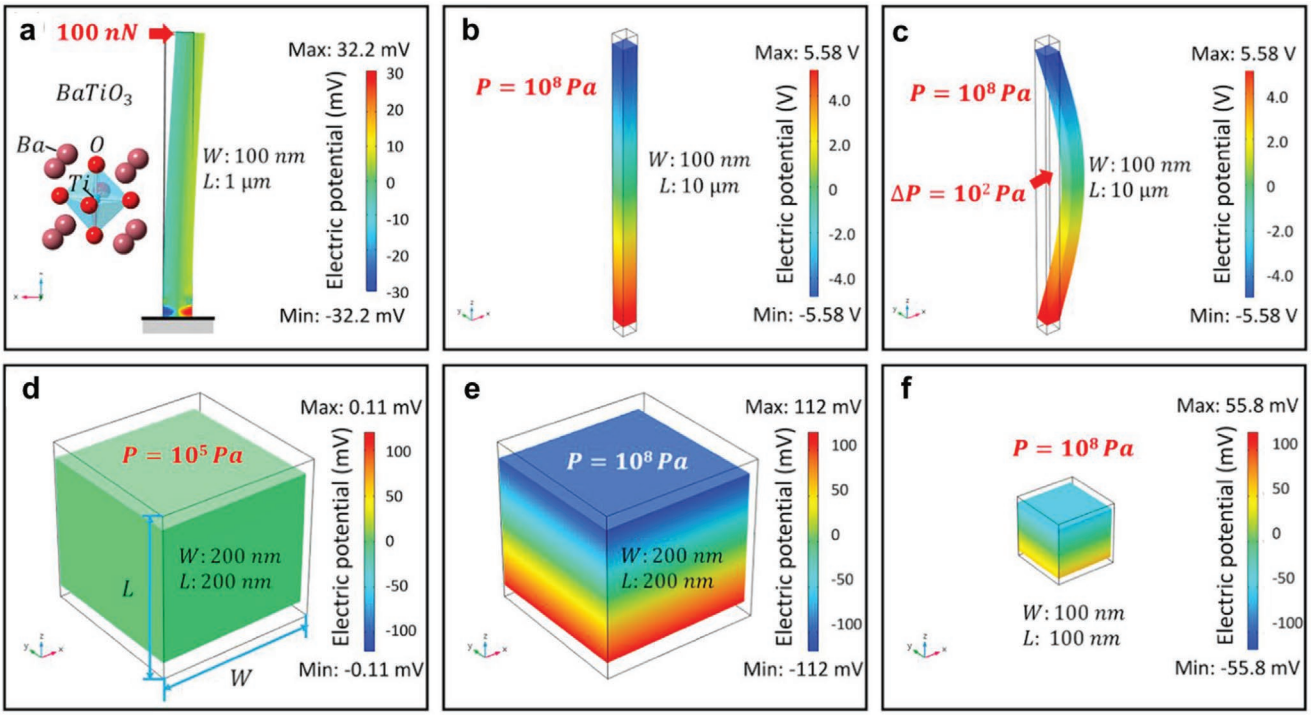

Figure 18. COMSOL simulation of the piezopotential distribution in $BaTiO_3$: a) FEM simulation for a lateral force on $BaTiO_3$ wire with fixed bottom; simulation for cavitation pressure results in b) an axial deformation and c) a lateral deformation of $BaTiO_3$ nanowire; $BaTiO_3$ nanoparticle under d) acoustic pressure and e) cavitation pressure; f) small-size nanoparticle under cavitation pressure. Reproduced with permission.[109] Copyright 2018, Elsevier.

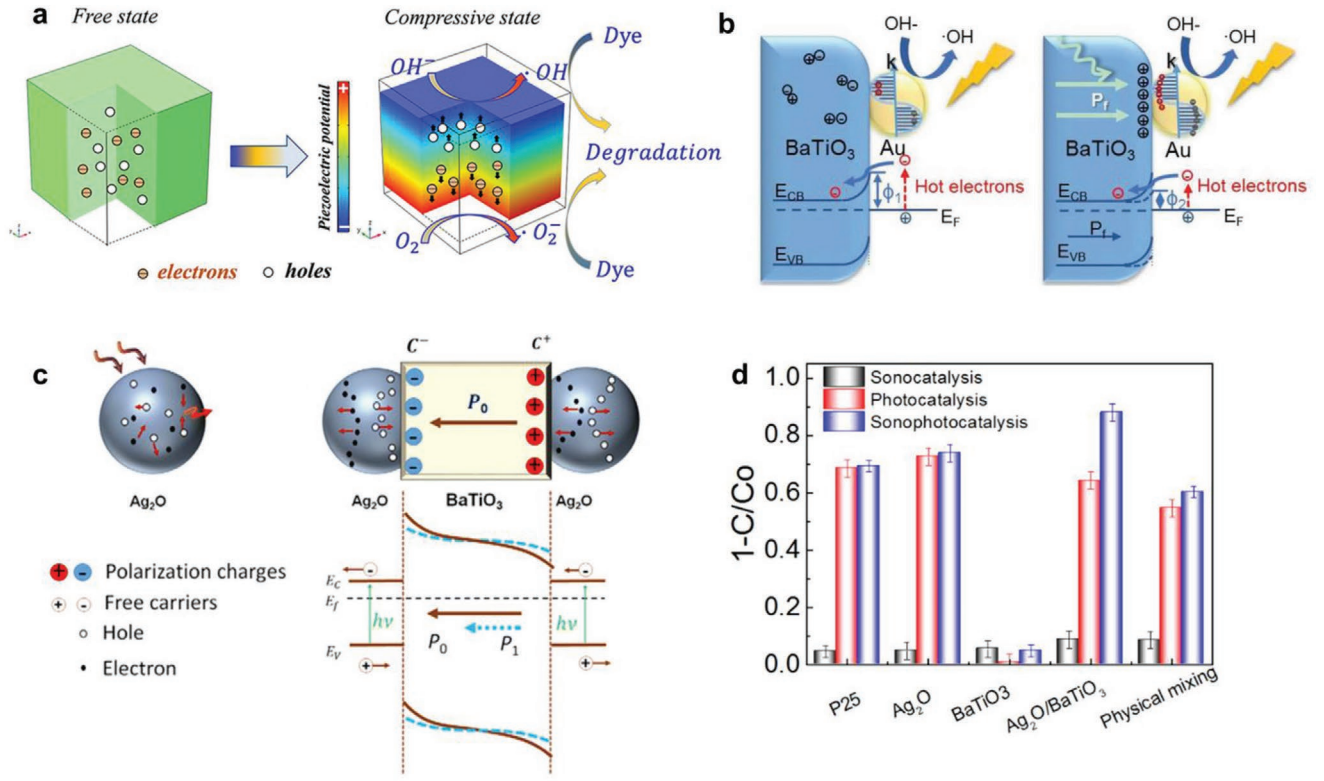

Figure 19. a) Proposed illustration of charge separation and redox reaction in the presence of piezopotential. Reproduced with permission.[115] Copyright 2018, American Chemical Society. b) Schematic illustration of the piezotronic-enhanced plasmonic photocatalysis mechanism. Reproduced with permission.[112] Copyright 2019, Wiley-VCH. c) Schematic illustration of charge generation and separation in Ag_2O attached to the two opposite surfaces of a $BaTiO_3$ nanocube that have opposite polarization charges due to piezoelectric effect. The solid line is the bands with spontaneous polarization charges; the dashed line indicates the decrease of the piezoelectric polarization with a mechanical strain. d) Sonocatalytic, photocatalytic, and sono-photocatalytic degradation of RhB for 1 h. Here sono(photo)catalytic should refer to the piezo(photo)catalytic process where piezopotential is induced by the pressure from ultrasonication. Reproduced with permission.[43] Copyright 2015, American Chemical Society.

photocatalysis, with the complete degradation of MO in 60 min (entry 7 in Table 3). Besides, Li et al. combined $BaTiO_3$ and Ag_2O semiconductor, and the spontaneous polarization potential of $BaTiO_3$ generated under ultrasonic wave significantly enhanced the photocatalytic activity of the Ag_2O–$BaTiO_3$ hybrid photocatalyst. The degradation efficiency of RhB is 100% in about 1.5 h with the relatively high cyclic performance (Figure 19c,d). All in all, it can be speculated that the synergistic coupling of piezocatalysis of $BaTiO_3$ and photocatalysis may create new inspirations and feasibilities for future photocatalysis.

In addition, piezoelectric effect was also used for disinfection. Feng et al. achieved prominent performance for the inactivation of *E. coli* when $BaTiO_3$ was stressed by ultrasound to generate piezopotential, attributed to the synergetic effect between piezocatalytic oxidation and mechanical destruction.[116]

Summaries of typical metal titanates (including the above-mentioned catalysts) on piezo-promoted photocatalytic and photoelectrocatalytic processes are listed in Table 3.

4.3.2. Polyvinylidene Fluoride

Organic ferroelectric materials usually have better flexibility than common inorganic piezo crystals. The β-phase PVDF with a high piezoelectric coefficient can be readily polarized through poling, stretching and thermal treatment.[120] Recently, PVDF with piezoelectric effect was proved to be an ideal candidate to generate a spatial electric field when combining with photocatalysts (**Figure 20**). The spatial piezoelectric field facilitates the photoinduced holes and electrons of TiO_2 to transfer toward the negative and positive potential surfaces of the PVDF–TiO_2 film (driven by the Coulomb force), respectively. Therefore, the piezo-photocatalytic degradation efficiency of rhodamine B is improved by about 55% compared with bare photocatalysis. And the corresponding first-order reaction rate constant k value is 5.42 times increased.[121]

4.4. Integration of Piezoelectric Semiconductors

The integration of two or more piezo-semiconductors into one heterojunction has shown significant promotion of photo(electro)catalytic performances. As shown in **Figure 21**, the synergetic effect of heterojunction and internal piezoelectric field is expected to greatly boost charge separation and migration.

As shown in **Figure 22**a,b, Jia et al. combined piezoelectric $KNbO_3$/MoS_2 for superior photocatalytic H_2 production and

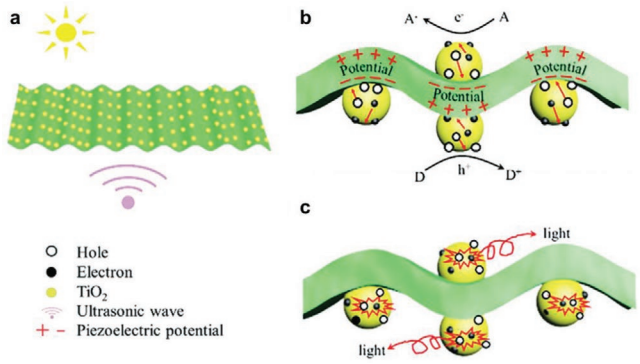

Figure 20. a) The mechanism of the built-in electric field enhanced photocatalytic performance over PVDF–TiO_2 composited film. b) Piezopotential is generated in the interface via deformation, and the charge separation of TiO_2 is accelerated. c) The deformation of (poly(dimethylsiloxane) (PDMS), without piezoelectric effects)—TiO_2 film cannot introduce potential, with the electrons and holes recombining. Reproduced with permission.[121] Copyright 2017, The Royal Society of Chemistry.

organic pollutant degradation.[78] In this $KNbO_3/MoS_2$ composite, MoS_2 acts as cocatalyst to transfer the photoinduced electrons and holes from $KNbO_3$ (black curve in Figure 22c). Moreover, under external strain, the deformation of $KNbO_3$ will lead to a large number of positive and negative polarization charges on the opposite surfaces. The steeper bending of energy band (blue curve in Figure 22c) will facilitate the transfer of photoinduced electrons and holes. Meanwhile few layer MoS_2 nanosheets are also easily deformed to create an additional piezoelectric potential, which further improves the photocatalytic performance. Consequently, the optimum H_2 production rate reaches 96 μmol g^{-1} h^{-1}, and the optimum RhB degradation efficiency reaches 95% in 4 h, which are respectively 2.0 and 3.7 times higher than those only under light irradiation. And the degradation efficiency (k) is about ten times higher than pure $KNbO_3$ and MoS_2.

Similarly, other binary piezo-semiconductor derivatives showed significant enhancement in catalytic performance, such

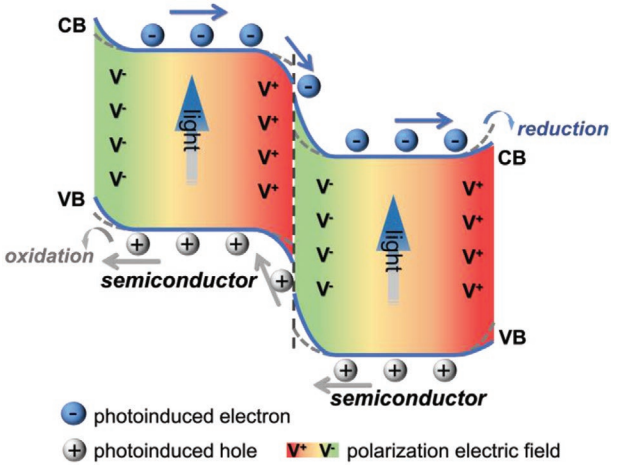

Figure 21. Schematic diagram of the integration mechanism of piezoelectric semiconductors. The gray dashed line represents the initial band edge without strain while the blue solid line represents the band edge under strain.

as p-MoS_2/n-type ZnO diode.[122] For multicomponent semiconductors, the piezo-catalytic performance depends on not only external strain but also the crystal phase and particle size. For example, the piezoelectric $BiFeO_3$–$PbTiO_3$ composite exhibits phase-dependent activities, among which the trapped metastable tetragonal phase is found to show the best photocatalytic activity as compared to its stable tetragonal- or rhombohedral-phase counterparts.[123] This work implies that the size effect can be exploited as an effective strategy for the manipulation of functional properties.

The construction of hybrid/hetero structures has been recognized as an effective route for high reaction efficiencies (usually higher than their pure counterparts). When one piezoelectric material is integrated with another semiconductor, not only charge transfer is facilitated but also more active sites are provided. Some recent works further focus on the integration of two or more piezoelectric materials into one heterojunction, which are promising in solar conversion. First, the coupled built-in electric field from contacted materials provides a stronger driving force to facilitate the overall charge transfer in designed directions; Second, the potential of surface band edge can be rationally modulated to provide more robust electrons/holes in redox reaction.

5. Summary and Perspective

Direct conversion of solar energy is an essential and indispensable research branch to alleviate the increasing fossil energy and environment crisis, however its efficiency is still far from satisfying. For this, piezo-phototronics-enhanced photo(electro) catalysis provides an ideal platform for the coupling utilization of ambient mechanical energy and solar light. And up to now, great advances have been achieved attributed to the unremitting endeavor of researchers. The core of these studies mainly lies in tuning the polarization-induced piezopotential toward favorable band bending and charge transfer kinetics. Recent works have revealed that piezo-catalysis is an ideal approach that enables the enhancement of electrochemical processes at both the bulk and surface by polarization charges, which promotes different kinds of carriers to move toward spatially different locations. Such controllable characteristics make piezo-phototronics very powerful to replenish traditional photocatalysis with new working principles, which needs multidisciplinary contributions. However, some fundamental questions regarding this research area still remain, such as the following:

i) Additional efforts in precise determination and comparison of the factors affecting piezo-phototronics, such as the thickness of space charge zone, defects at the interface and contact potential (Schottky barrier) of heterostructures are needed. And understanding of the piezoelectric properties of 3D materials in addition to 1 or 2D structures is the key factor in novel-catalyst design.
ii) Controllable delivery of external strain/stress on semiconductor toward piezotronic or piezo-phototronic effect is needed. For example, the height of Schottky barrier can be unidirectionally modulated by changing the external strain or stress, thus the charge transfer pathway and migration kinetics can

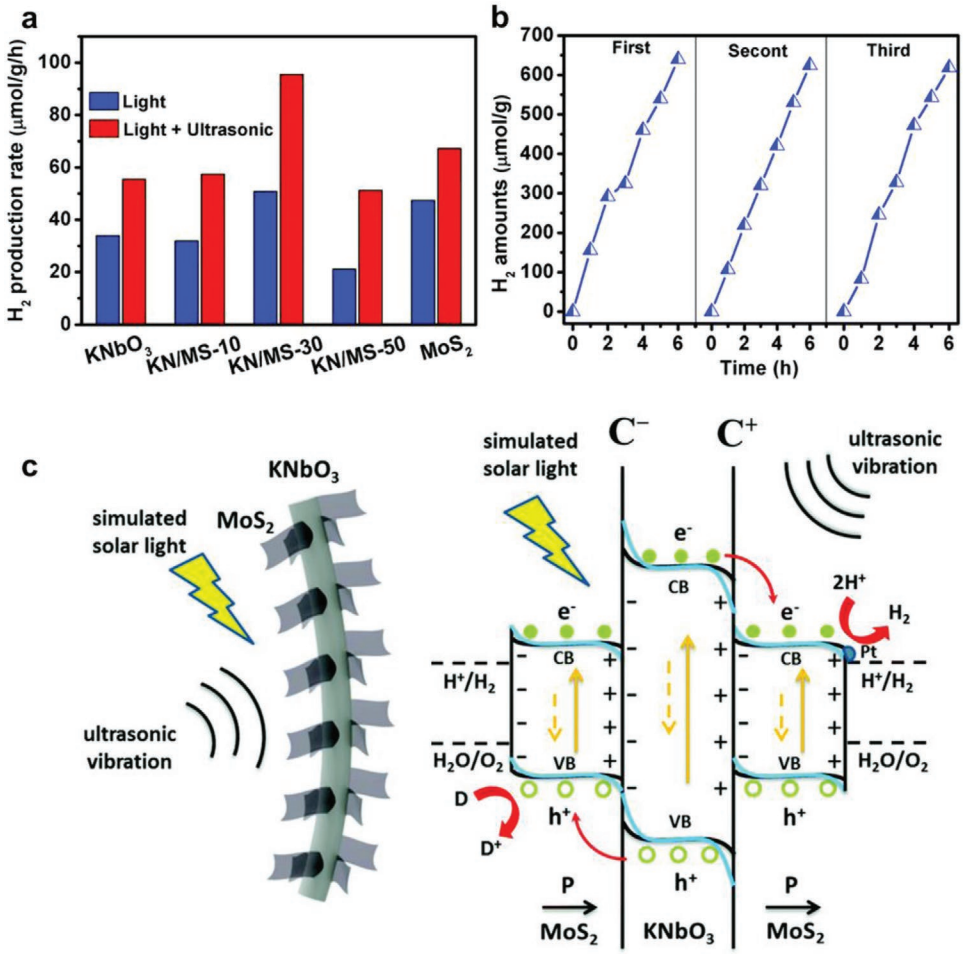

Figure 22. a) Comparison of H_2 evolution rate under different conditions. b) Cycling test under piezopotential (by ultrasonic vibration) and simulated solar-light irradiation. c) Schematic illustration of the piezo-enhanced photocatalytic mechanism of $KNbO_3/MoS_2$. Reproduced with permission.[78] Copyright 2019, The Royal Society of Chemistry.

be controlled. Meanwhile the accompanying change in redox capability of charges can affect the redox kinetics. Moreover, an internal coupling of piezotronic and photocatalytic process toward the optimization of catalytic performance remains a complex task.

iii) The real-time analyses of the piezo-phototronic processes (carrier generation, separation, and recombination tuned by piezoelectric charges) through in situ measurements are of crucial importance in identifying the electron transfer and reaction pathway.

iv) Understanding and application of this long-overlooked research area give rise to new fundamental phenomena and unprecedented photoelectrochemical materials. However, only a few piezotronic semiconductors have been successfully adopted in photo(electro)catalysis. The construction and design of more semiconductors (like plasma photocatalysts and multicomponent composites) with tunable properties are necessary. Also, most reports mainly focus on the limited reactions of water splitting and organic degradation up to now, the application of piezo-phototronics in additional aspects including CO_2 reduction, H_2O_2 production and nitrogen fixation are all highly anticipated in the environmental and energy fields.

v) Since both photocatalytic and photoelectrochemical processes are highly temperature-dependent, the utilization of piezo-phototronics to energy conversion from temperature fluctuations needs more careful studies in a range of operating environments. Detailed designs that considering temperature gradients when generating mechanical strain to enhance the pyroelectric coefficients are also of interest.

vi) Exploration of new materials are important for enhancing the piezophotocatalysis process. 2D materials, especially single-layered 2D materials that have strong piezoelectricity, provides a new system, which deserves to be synthesized and investigated.

vii) We anticipate that the (electro)catalysis can occur even without photon, such as in the unilluminated surface. Therefore, the respective functionality of synchronous piezocatalysis and piezo-photocatalysis during water splitting or degradation should be focused and investigated.

Acknowledgements

L.P. and S.S. contributed equally to this work. The authors appreciate the supports from the National Natural Science Foundation of China

(21978200, 21676193) and the Scientific Research Projects of the Ministry of Education of China (6141A02033522).

Conflict of Interest

The authors declare no conflict of interest.

Keywords

photocatalysis, photoelectrocatalysis, piezo-phototronic effect, piezopotential

Received: January 18, 2020
Revised: February 16, 2020
Published online:

[1] a) Q. Wang, K. Domen, *Chem. Rev.* **2020**, *120*, 919; b) S. S. Chen, T. Takata, K. Domen, *Nat. Rev. Mater.* **2017**, *2*, 17050; c) S. Sun, G. Shen, J. Jiang, W. Mi, X. Liu, L. Pan, X. Zhang, J.-J. Zou, *Adv. Energy Mater.* **2019**, *9*, 1901505; d) L. Pan, M. Ai, C. Huang, L. Yin, X. Liu, R. Zhang, S. Wang, Z. Jiang, X. Zhang, J.-J. Zou, W. Mi, *Nat. Commun.* **2020**, *11*, 418.
[2] X. Wang, J. Song, J. Liu, Z. L. Wang, *Science* **2007**, *316*, 102.
[3] A. Fujishima, K. Honda, *Nature* **1972**, *238*, 37.
[4] P. Zhou, J. Yu, M. Jaroniec, *Adv. Mater.* **2014**, *26*, 4920.
[5] X. T. Xu, L. Pan, X. Zhang, L. Wang, J.-J. Zou, *Adv. Sci.* **2019**, *6*, 1801505.
[6] a) M. B. Starr, X. D. Wang, *Nano Energy* **2015**, *14*, 296; b) X. Han, L. Kou, X. Lang, J. Xia, N. Wang, R. Qin, J. Lu, J. Xu, Z. Liao, X. Zhang, X. Shan, X. Song, J. Gao, W. Guo, D. Yu, *Adv. Mater.* **2009**, *21*, 4937; c) Y. Gao, Z. L. Wang, *Nano Lett.* **2007**, *7*, 2499; d) Z. L. Wang, *Adv. Mater.* **2007**, *19*, 889.
[7] W. Z. Wu, Z. L. Wang, *Nat. Rev. Mater.* **2016**, *1*, 16031.
[8] Y. Qin, X. Wang, Z. L. Wang, *Nature* **2009**, *457*, 340.
[9] L. Zhu, Z. L. Wang, *Adv. Funct. Mater.* **2019**, *29*, 1808214.
[10] Y. Zhang, Y. S. Leng, M. Willatzen, B. L. Huang, *MRS Bull.* **2018**, *43*, 928.
[11] a) C. R. Bowen, H. A. Kim, P. M. Weaver, S. Dunn, *Energy Environ. Sci.* **2014**, *7*, 25; b) Z. L. Wang, *Mater. Today* **2007**, *10*, 20.
[12] Z. L. Wang, W. Z. Wu, C. Falconi, *MRS Bull.* **2018**, *43*, 922.
[13] Z. L. Wang, *Nano Today* **2010**, *5*, 540.
[14] C. Pan, J. Zhai, Z. L. Wang, *Chem. Rev.* **2019**, *119*, 9303.
[15] Y. Liu, Y. Zhang, Q. Yang, S. M. Niu, Z. L. Wang, *Nano Energy* **2015**, *14*, 257.
[16] Z. L. Wang, *Adv. Mater.* **2012**, *24*, 4632.
[17] X. N. Wen, W. Z. Wu, C. F. Pan, Y. F. Hu, Q. Yang, Z. L. Wang, *Nano Energy* **2015**, *14*, 276.
[18] a) Q. Yang, W. Wang, S. Xu, Z. L. Wang, *Nano Lett.* **2011**, *11*, 4012; b) Z. L. Wang, J. Song, *Science* **2006**, *312*, 242.
[19] Z. Gao, J. Zhou, Y. Gu, P. Fei, Y. Hao, G. Bao, Z. L. Wang, *J. Appl. Phys.* **2009**, *105*, 113707.
[20] a) X. Wang, J. Zhou, J. Song, J. Liu, N. Xu, Z. L. Wang, *Nano Lett.* **2006**, *6*, 2768; b) J. H. He, C. L. Hsin, J. Liu, L. J. Chen, Z. L. Wang, *Adv. Mater.* **2007**, *19*, 781.
[21] Y. Zhang, W. Jie, P. Chen, W. Liu, J. Hao, *Adv. Mater.* **2018**, *30*, 1707007.
[22] R. Yu, L. Dong, C. Pan, S. Niu, H. Liu, W. Liu, S. Chua, D. Chi, Z. L. Wang, *Adv. Mater.* **2012**, *24*, 3532.
[23] Y. Zhang, Y. Liu, Z. L. Wang, *Adv. Mater.* **2011**, *23*, 3004.
[24] D. Tan, Y. Xiang, Y. G. Leng, Y. S. Leng, *Nano Energy* **2018**, *50*, 291.
[25] L. P. Zhu, Z. L. Wang, *J. Phys. D: Appl. Phys.* **2019**, *52*, 343001.
[26] Y. Chen, L. Wang, R. J. Gao, Y. C. Zhang, L. Pan, C. Y. Huang, K. Liu, X. Y. Chang, X. W. Zhang, J.-J. Zou, *Appl. Catal., B* **2019**, *259*, 118079.
[27] H. Li, W. Tu, Y. Zhou, Z. Zou, *Adv. Sci.* **2016**, *3*, 1500389.
[28] F. Chen, H. Huang, L. Guo, Y. Zhang, T. Ma, *Angew. Chem., Int. Ed.* **2019**, *58*, 10061.
[29] Y. W. Feng, L. L. Ling, Y. X. Wang, Z. M. Xu, F. L. Cao, H. X. Li, Z. F. Bian, *Nano Energy* **2017**, *40*, 481.
[30] Z. Liang, C. F. Yan, S. Rtimi, J. Bandara, *Appl. Catal., B* **2019**, *241*, 256.
[31] T. Zhang, W. Lei, P. Liu, J. A. Rodriguez, J. Yu, Y. Qi, G. Liu, M. Liu, *Chem. Sci.* **2015**, *6*, 4118.
[32] a) D. Jiang, Z. Sun, H. Jia, D. Lu, P. Du, *J. Mater. Chem. A* **2016**, *4*, 675; b) R. Baron, C. H. Huang, D. M. Bassani, A. Onopriyenko, M. Zayats, I. Willner, *Angew. Chem., Int. Ed.* **2005**, *44*, 4010.
[33] X. L. Xu, Z. Wu, L. B. Xiao, Y. M. Jia, J. P. Ma, F. F. Wang, L. Wang, M. S. Wang, H. T. Huang, *J. Alloys Compd.* **2018**, *762*, 915.
[34] Y. Hu, Y. Chang, P. Fei, R. L. Snyder, Z. L. Wang, *ACS Nano* **2010**, *4*, 1234.
[35] S. Niu, Y. Hu, X. Wen, Y. Zhou, F. Zhang, L. Lin, S. Wang, Z. L. Wang, *Adv. Mater.* **2013**, *25*, 3701.
[36] Y. C. Wang, J. M. Wu, *Adv. Funct. Mater.* **2020**, *30*, 1907619.
[37] J. P. Ma, J. Ren, Y. M. Jia, Z. Wu, L. Chen, N. O. Haugen, H. T. Huang, Y. S. Liu, *Nano Energy* **2019**, *62*, 376.
[38] X. Yu, S. Wang, X. Zhang, A. Qi, X. Qiao, Z. Liu, M. Wu, L. Li, Z. L. Wang, *Nano Energy* **2018**, *46*, 29.
[39] J. M. Wu, W. E. Chang, Y. T. Chang, C. K. Chang, *Adv. Mater.* **2016**, *28*, 3718.
[40] L. Wang, S. Liu, Z. Wang, Y. Zhou, Y. Qin, Z. L. Wang, *ACS Nano* **2016**, *10*, 2636.
[41] D. F. Yu, Z. H. Liu, J. M. Zhang, S. Li, Z. C. Zhao, L. F. Zhu, W. S. Liu, Y. H. Lin, H. Liu, Z. T. Zhang, *Nano Energy* **2019**, *58*, 695.
[42] a) P. Lin, C. Pan, Z. L. Wang, *Mater. Today Nano* **2018**, *4*, 17; b) Y. Peng, M. Que, J. Tao, X. Wang, J. Lu, G. Hu, B. Wan, Q. Xu, C. Pan, *2D Mater.* **2018**, *5*, 042003.
[43] H. Li, Y. Sang, S. Chang, X. Huang, Y. Zhang, R. Yang, H. Jiang, H. Liu, Z. L. Wang, *Nano Lett.* **2015**, *15*, 2372.
[44] Z. L. Wang, *Piezotronics and Piezo-Phototronics*, Springer, Berlin, Heidelberg **2012**.
[45] T. Yang, J. Xue, H. Tan, A. Xie, S. Li, W. Yan, Y. Shen, *J. Mater. Chem. A* **2018**, *6*, 1210.
[46] Z. J. Wang, T. C. Hu, H. X. He, Y. M. Fu, X. Zhang, J. Sun, L. L. Xing, B. D. Liu, Y. Zhang, X. Y. Xue, *ACS Sustainable Chem. Eng.* **2018**, *6*, 10162.
[47] W. S. Tong, Y. H. Zhang, H. W. Huang, K. Xiao, S. X. Yu, Y. Zhou, L. P. Liu, H. T. Li, L. Liu, T. Huang, M. Li, Q. Zhang, R. F. Du, Q. An, *Nano Energy* **2018**, *53*, 513.
[48] H. Zou, X. Li, W. Peng, W. Wu, R. Yu, C. Wu, W. Ding, F. Hu, R. Liu, Y. Zi, Z. L. Wang, *Adv. Mater.* **2017**, *29*, 1701412.
[49] J. Sun, X. Zhang, Y. Lang, J. Bian, R. Gao, P. Li, Y. Wang, C. Li, *Nano Energy* **2017**, *32*, 96.
[50] D. Hong, W. Zang, X. Guo, Y. Fu, H. He, J. Sun, L. Xing, B. Liu, X. Xue, *ACS Appl. Mater. Interfaces* **2016**, *8*, 21302.
[51] C. Sun, Y. M. Fu, Q. Wang, L. L. Xing, B. D. Liu, X. Y. Xue, *RSC Adv.* **2016**, *6*, 87446.
[52] Y. Ye, K. Q. Wang, X. Y. Huang, R. Lei, Y. Zhao, P. Liu, *Catal. Sci. Technol.* **2019**, *9*, 3771.
[53] X. Y. Chen, L. F. Liu, Y. W. Feng, L. F. Wang, Z. F. Bian, H. X. Li, Z. L. Wang, *Mater. Today* **2017**, *20*, 501.
[54] H. Li, Y. Yu, M. B. Starr, Z. Li, X. Wang, *J. Phys. Chem. Lett.* **2015**, *6*, 3410.
[55] J. Shi, M. B. Starr, H. Xiang, Y. Hara, M. A. Anderson, J. H. Seo, Z. Ma, X. Wang, *Nano Lett.* **2011**, *11*, 5587.
[56] X. Y. Xue, W. L. Zang, P. Deng, Q. Wang, L. L. Xing, Y. Zhang, Z. L. Wang, *Nano Energy* **2015**, *13*, 414.

[57] Y. Bai, J. Z. Zhao, Z. L. Lv, K. Lu, *Ceram. Int.* **2019**, *45*, 15065.
[58] J. H. Chang, H. N. Lin, *Mater. Lett.* **2014**, *132*, 134.
[59] Z. Kang, H. Si, S. Zhang, J. Wu, Y. Sun, Q. Liao, Z. Zhang, Y. Zhang, *Adv. Funct. Mater.* **2019**, *29*, 1808032.
[60] K. S. Hong, H. F. Xu, H. Konishi, X. C. Li, *J. Phys. Chem. Lett.* **2010**, *1*, 997.
[61] Y. Dai, C. Wu, Z. Wu, Z. Zhao, L. Li, Y. Lu, Z. L. Wang, *Adv. Sci.* **2019**, *6*, 1900314.
[62] L. Zhu, L. Wang, F. Xue, L. Chen, J. Fu, X. Feng, T. Li, Z. L. Wang, *Adv. Sci.* **2017**, *4*, 1600185.
[63] Y. X. Li, Z. M. Zhang, W. H. Han, C. J. Jiang, E. Q. Xie, *Nano Energy* **2017**, *36*, 118.
[64] Y. Z. Zhang, X. L. Huang, J. Yeom, *Nano-Micro Lett.* **2019**, *11*, 11.
[65] X. Xu, Y. Jia, L. Xiao, Z. Wu, *Chemosphere* **2018**, *193*, 1143.
[66] Y. Zhang, C. H. Liu, G. L. Zhu, X. Huang, W. Liu, W. G. Hu, M. Song, W. D. He, J. Liu, J. Y. Zhai, *RSC Adv.* **2017**, *7*, 48176.
[67] L. L. Zhang, D. Zhu, H. X. He, Q. Wang, L. L. Xing, X. Y. Xue, *J. Phys. Chem. Solids* **2017**, *102*, 27.
[68] A. Sarkar, A. K. Katiyar, S. Mukherjee, S. K. Ray, *J. Phys. D: Appl. Phys.* **2017**, *50*, 145104.
[69] H. You, Z. Wu, Y. Jia, X. Xu, Y. Xia, Z. Han, Y. Wang, *Chemosphere* **2017**, *183*, 528.
[70] Z. F. Liu, Q. J. Cai, C. H. Ma, J. Zhang, J. Q. Liu, *New J. Chem.* **2017**, *41*, 7947.
[71] H. Wang, X. Liu, S. L. Wang, L. Li, *Appl. Catal., B* **2018**, *222*, 209.
[72] K. Wang, Z. Fang, X. Huang, W. Feng, Y. Wang, B. Wang, P. Liu, *Chem. Commun.* **2017**, *53*, 9765.
[73] Y. T. Hong, J. P. Ma, Z. Wu, J. S. Ying, H. L. You, Y. M. Jia, *Acta Phys. Sin.* **2018**, *67*, 107702.
[74] a) T. T. A. Lummen, J. Leung, A. Kumar, X. Wu, Y. Ren, B. K. VanLeeuwen, R. C. Haislmaier, M. Holt, K. Lai, S. V. Kalinin, V. Gopalan, *Adv. Mater.* **2017**, *29*, 1700530; b) P. G. Kang, T. K. Lee, C. W. Ahn, I. W. Kim, H. H. Lee, S. B. Choi, K. D. Sung, J. H. Jung, *Nano Energy* **2015**, *17*, 261.
[75] S. Singh, N. Khare, *Nano Energy* **2017**, *38*, 335.
[76] S. Singh, N. Khare, *Nano Energy* **2017**, *42*, 173.
[77] Q.-P. Ding, Y.-P. Yuan, X. Xiong, R.-P. Li, H.-B. Huang, Z.-S. Li, T. Yu, Z.-G. Zou, S.-G. Yang, *J. Phys. Chem. C* **2008**, *112*, 18846.
[78] S. Jia, Y. Su, B. Zhang, Z. Zhao, S. Li, Y. Zhang, P. Li, M. Xu, R. Ren, *Nanoscale* **2019**, *11*, 7690.
[79] S. S. Wang, Z. Wu, J. Chen, J. P. Ma, J. S. Ying, S. C. Cui, S. G. Yu, Y. M. Hu, J. H. Zhao, Y. M. Jia, *Ceram. Int.* **2019**, *45*, 11703.
[80] a) C. Pan, S. Niu, Y. Ding, L. Dong, R. Yu, Y. Liu, G. Zhu, Z. L. Wang, *Nano Lett.* **2012**, *12*, 3302; b) D. Shvydka, J. Drayton, A. D. Compaan, V. G. Karpov, *Appl. Phys. Lett.* **2005**, *87*, 123505.
[81] Y. Zhao, Z. B. Fang, W. H. Feng, K. Q. Wang, X. Y. Huang, P. Liu, *ChemCatChem* **2018**, *10*, 3397.
[82] Y. S. Zhou, K. Wang, W. Han, S. C. Rai, Y. Zhang, Y. Ding, C. Pan, F. Zhang, W. Zhou, Z. L. Wang, *ACS Nano* **2012**, *6*, 6478.
[83] D. Cao, Z. Wang, Nasori, L. W , Y. Mi, Y. Lei, *Angew. Chem., Int. Ed.* **2014**, *53*, 11027.
[84] Y. L. Liu, J. M. Wu, *Nano Energy* **2019**, *56*, 74.
[85] S. C. Tu, Y. H. Zhang, A. H. Reshak, S. Auluck, L. Q. Ye, X. P. Han, T. Y. Ma, H. W. Huang, *Nano Energy* **2019**, *56*, 840.
[86] Y.-T. Wang, K.-S. Chang, R. J. Xie, *J. Am. Ceram. Soc.* **2016**, *99*, 2593.
[87] H. M. Lin, K. S. Chang, *RSC Adv.* **2017**, *7*, 30513.
[88] D. Shao, L. Zhang, S. Sun, W. Wang, *ChemSusChem* **2018**, *11*, 527.
[89] a) L. Liu, J. Wu, L. Wu, M. Ye, X. Liu, Q. Wang, S. Hou, P. Lu, L. Sun, J. Zheng, L. Xing, L. Gu, X. Jiang, L. Xie, L. Jiao, *Nat. Mater.* **2018**, *17*, 1108; b) J. Shi, *Chem* **2017**, *2*, 468.
[90] L. Yin, X. Hai, K. Chang, F. Ichihara, J. Ye, *Small* **2018**, *14*, 1704153.
[91] H. Zhu, Y. Wang, J. Xiao, M. Liu, S. Xiong, Z. J. Wong, Z. Ye, Y. Ye, X. Yin, X. Zhang, *Nat. Nanotechnol.* **2015**, *10*, 151.
[92] S. Li, Z. Zhao, D. Yu, J.-Z. Zhao, Y. Su, Y. Liu, Y. Lin, W. Liu, H. Xu, Z. Zhang, *Nano Energy* **2019**, *66*, 104083.
[93] J. M. Wu, Y. G. Sun, W. E. Chang, J. T. Lee, *Nano Energy* **2018**, *46*, 372.
[94] W. Wu, L. Wang, R. Yu, Y. Liu, S. H. Wei, J. Hone, Z. L. Wang, *Adv. Mater.* **2016**, *28*, 8463.
[95] H. Y. Zhang, J. D. Dai, C. M. Liu, *Mater. Res. Express* **2019**, *6*, 025025.
[96] T. M. Chou, S. W. Chan, Y. J. Lin, P. K. Yang, C. C. Liu, Y. J. Lin, J. M. Wu, J. T. Lee, Z. H. Lin, *Nano Energy* **2019**, *57*, 14.
[97] S. Masimukku, Y. C. Hu, Z. H. Lin, S. W. Chan, T. M. Chou, J. M. Wu, *Nano Energy* **2018**, *46*, 338.
[98] a) P. Lin, L. P. Zhu, D. Li, L. Xu, C. F. Pan, Z. L. Wang, *Adv. Funct. Mater.* **2018**, *28*, 1802849; b) M. H. Wu, J. T. Lee, Y. J. Chung, M. Srinivaas, J. M. Wu, *Nano Energy* **2017**, *40*, 369.
[99] G. Eda, H. Yamaguchi, D. Voiry, T. Fujita, M. Chen, M. Chhowalla, *Nano Lett.* **2011**, *11*, 5111.
[100] S. Anand, K. Thekkepat, U. V. Waghmare, *Nano Lett.* **2016**, *16*, 126.
[101] W. Liu, X. Ren, *Phys. Rev. Lett.* **2009**, *103*, 257602.
[102] M. Acosta, N. Novak, V. Rojas, S. Patel, R. Vaish, J. Koruza, G. A. Rossetti, J. Rodel, *Appl. Phys. Rev.* **2017**, *4*, 041305.
[103] K. I. Park, S. Xu, Y. Liu, G. T. Hwang, S. J. Kang, Z. L. Wang, K. J. Lee, *Nano Lett.* **2010**, *10*, 4939.
[104] G. Cilaveni, K. V. A. Kumar, S. S. K. Raavi, C. Subrahmanyam, S. Asthana, *J. Alloys Compd.* **2019**, *798*, 540.
[105] S. C. Tu, H. W. Huang, T. R. Zhang, Y. H. Zhanga, *Appl. Catal., B* **2017**, *219*, 550.
[106] L. M. Guo, C. F. Zhong, J. Q. Cao, Y. N. Hao, M. Lei, K. Bi, Q. J. Sun, Z. L. Wang, *Nano Energy* **2019**, *62*, 513.
[107] W. Yang, Y. Yu, M. B. Starr, X. Yin, Z. Li, A. Kvit, S. Wang, P. Zhao, X. Wang, *Nano Lett.* **2015**, *15*, 7574.
[108] Z. R. Liu, L. W. Wang, X. Yu, J. Zhang, R. Q. Yang, X. D. Zhang, Y. C. Ji, M. Q. Wu, L. Deng, L. L. Li, Z. L. Wang, *Adv. Funct. Mater.* **2019**, *29*, 1807279.
[109] J. Wu, N. Qin, D. H. Bao, *Nano Energy* **2018**, *45*, 44.
[110] W. Lv, L. J. Kong, S. Y. Lan, J. X. Feng, Y. Xiong, S. H. Tian, *J. Chem. Technol. Biotechnol.* **2017**, *92*, 152.
[111] S. Y. Xu, Z. H. Liu, M. L. Zhang, L. M. Guo, *J. Alloys Compd.* **2019**, *801*, 483.
[112] S. Y. Xu, L. M. Guo, Q. J. Sun, Z. L. Wang, *Adv. Funct. Mater.* **2019**, *29*, 1808737.
[113] J. X. Feng, J. X. Sun, X. S. Liu, J. Z. Zhu, Y. Xiong, S. H. Tian, *Environ. Sci.: Nano* **2019**, *6*, 2241.
[114] X. Zhou, S. Wu, C. Li, F. Yan, H. Bai, B. Shen, H. Zeng, J. Zhai, *Nano Energy* **2019**, *66*, 104127.
[115] J. Wu, Q. Xu, E. Lin, B. Yuan, N. Qin, S. K. Thatikonda, D. Bao, *ACS Appl. Mater. Interfaces* **2018**, *10*, 17842.
[116] J. X. Feng, Y. Fu, X. S. Liu, S. H. Tian, S. Y. Lan, Y. Xiong, *ACS Sustainable Chem. Eng.* **2018**, *6*, 6032.
[117] I. C. Amaechi, A. Hadj Youssef, G. Kolhatkar, D. Rawach, C. Gomez-Yañez, J. P. Claverie, S. Sun, A. Ruediger, *Catal. Today* **2019**, https://doi.org/10.1016/j.cattod.2019.07.021.
[118] C. Chao, Y. Zhou, T. Han, Y. Yang, J. Wei, H. Li, W. He, *J. Alloys Compd.* **2020**, *825*, 154060.
[119] B. Yang, C. Wu, J. Wang, J. Bian, L. Wang, M. Liu, Y. Du, Y. Yang, *Ceram. Int.* **2020**, *46*, 4248.
[120] a) N. Jia, Q. Xing, G. Xia, J. Sun, R. Song, W. Huang, *Mater. Lett.* **2015**, *139*, 212; b) Y. L. Zhao, Q. L. Liao, G. J. Zhang, Z. Zhang, Q. J. Liang, X. Q. Liao, Y. Zhang, *Nano Energy* **2015**, *11*, 719.
[121] B. Y. Dai, H. M. Huang, W. Wang, Y. K. Chen, C. H. Lu, J. H. Kou, L. Z. Wang, F. L. Wang, Z. Z. Xu, *Catal. Sci. Technol.* **2017**, *7*, 5594.
[122] F. Xue, L. Chen, J. Chen, J. Liu, L. Wang, M. Chen, Y. Pang, X. Yang, G. Gao, J. Zhai, Z. L. Wang, *Adv. Mater.* **2016**, *28*, 3391.
[123] B. Narayan, S. Adhikari, G. Madras, R. Ranjan, *Phys. Rev. Appl.* **2017**, *7*, 024018.